Master Project, Fall semester 2013 – 2014, Micro-engineering

Gallium and Boron Doping of Amorphous Silicon for Solar Cells

Nil ALMAT

Professor Christophe Ballif
Supervisor Franz-Josef Haug
Assistant Michael Stuckelberger

Photovoltaics and Thin-film Electronics Labratory (PV-Lab)
Institute of Microengineering (IMT)
École Polytechnique Fédérale de Lausanne (EPFL)

January 17, 2014

Project description

The conversion efficiency of solar cells based on hydrogenated amorphous silicon degrades under light illumination. While part of this degradation is attributed to the intrinsic bulk properties of amorphous silicon, also the boron-doped amorphous silicon carbide layer contributes to the degradation. Further, boron diffusion into the bulk material during bulk deposition gives constraints in deposition conditions, mainly limiting deposition temperature. In order to overcome the limitations by boron-doped layers, the new dopant gallium shall be tested for its possible application by replacing boron in p-doped amorphous silicon layers. The goal of this project is therefore to develop p-doped amorphous silicon layers by plasma-enhanced chemical vapour deposition using trimethylgallium instead of trimethylboron, and to characterize these layers electrically and optically. Further, these layers shall directly be incorporated into solar cells to test their behaviour in actual devices in direct comparison with classically deposited cells containing boron.

Abstract

A possibility to increase the conversion efficiency of amorphous silicon solar cells is the increase of the deposition temperature of the absorber layer. However, this leads to poor charge collection of short-wavelength light known as boron-tailing. The mechanism behind is not completely clear, but boron diffusion might play an important role.

In this work, therefore, a new type of p-doping, trimethylgallium (TMGa), is compared to the most often used trimethylboron (TMB). Other gas precursors of the p-layers are silane, methane, and hydrogen.

First, different p-layer series with each dopant were fabricated by plasma enhanced chemical vapor deposition (PECVD) and characterized electrically and optically by dark conductivity measurements to determine the activation energy and by ellipsometry to deduce the band gap energy. The p-layer series were then incorporated in amorphous silicon p-i-n solar cells deposited by PECVD to observe the consequences of already obtained layer results. The solar cells were characterized by current-voltage and external quantum efficiency (EQE) measurements.

For the conducted layer and cell series, the following p-layer deposition parameters were varied: power, temperature, as well as, silane, methane, and dopant gas flows. Furthermore, for solar cell series i-layer deposition temperature and p-layer thickness studies were realized.

In general, series with gallium doped layers showed the same trends as those with boron-doped layers. However, significant differences could be observed. Namely, the energy band gap drops much stronger with increasing dopant concentration for gallium, which goes together with a stronger decrease of the activation energy (see figure a)

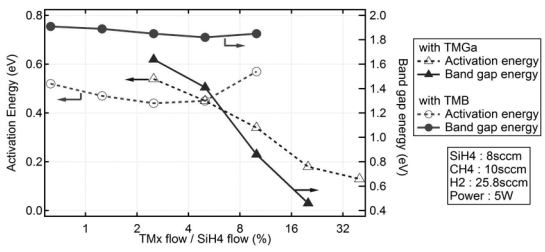

Figure a) Activation energy and band gapp-(a-SiC:H) layers doped by TMGa or TMB

This is in full agreement with the solar cell results as shown by the decreasing open-circuit voltage that is limited in this case by the p-layer band gap and with the EQE curves (shown in figures b and c)

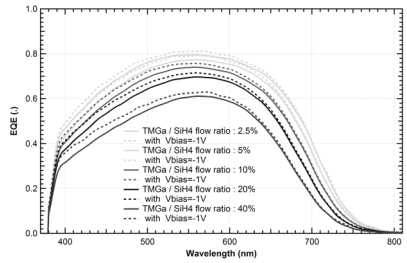

Figure b) External quantum efficiency of p-i-n solar cells with p-(a-SiC:H) layers doped by TMGa

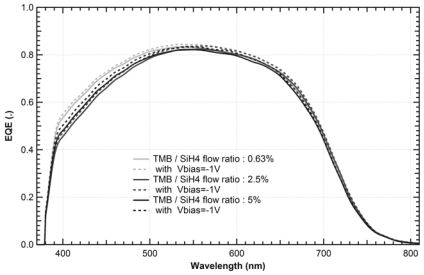

Figure c) External quantum efficiency of p-i-n solar cells with p-(a-SiC:H) layers doped by TMB

Mainly due to the limitations of band gap narrowing in case of gallium doping, boron doped layers lead in most cases to better solar cell performance. However, these experiments were limited by the mass flow controller of TMGa, not allowing for as low TMGa flows as TMB.

The best open circuit voltage (V_{OC}) obtained with solar cells containing gallium is 778.8 mV. Together with a short-circuit current (Jsc) of 14.60 mA/cm^2 and a fill factor of 46.21 %, the solar cell efficiency (η) of this cell was 5.83 %. For comparison, the same deposition conditions but with TMB resulted in solar cells with V_{OC}=924 mV, J_{SC} = 14.94 mA/cm^2, FF = 72.99 %, and η = 10.60 %.

Table of contents

1. Introduction

Enhanced sensibilization of people for pollution and energy consumption increased the need to minimize the use of fossil energy sources and to look for alternatives. Further, decisions to quit nuclear energy in most countries of Europe reinforce the research and development considering renewable energy technologies. Some of the most important energy sources available free-of-charge on Earth are geothermal, biomass, hydrolic, wind and solar. The latter provides the highest power and is available in every country at different extent.

The highest conversion efficiencies of solar cells are reported in [Green, 2013]. Numerous research groups all over the world work on further increase of the conversion efficiencies by studying new materials, designs, and production techniques.

Thanks to improvements and cost reductions made, photovoltaic modules have become more and more interesting products for private installations as well as for industrial electricity generation. In particular, Switzerland is one of the most contributing countries on the progress of photovoltaic technology. Sold solar modules have almost reached 250’000 in 2012 (see fiigure 1 a)) and the energy production passed 300 GWh as anounced by Swiss Federal Office of Energy according to statistc made by Swissolar [SFOE, 2013] (see figure 1 b)).

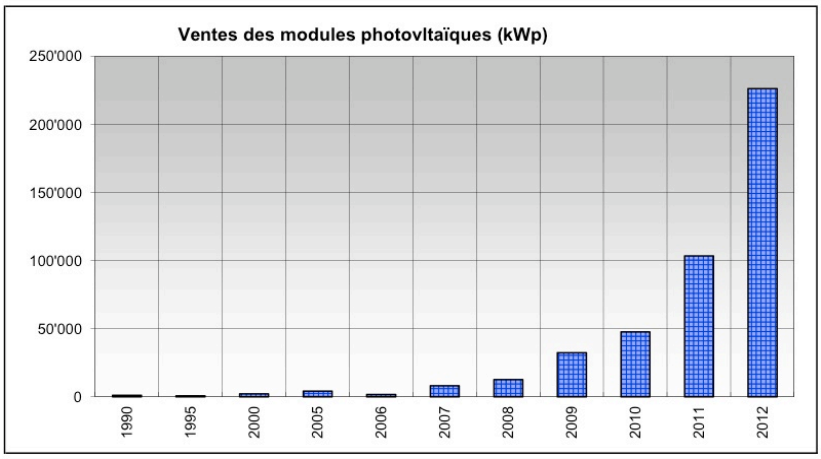

a) Solar module sales

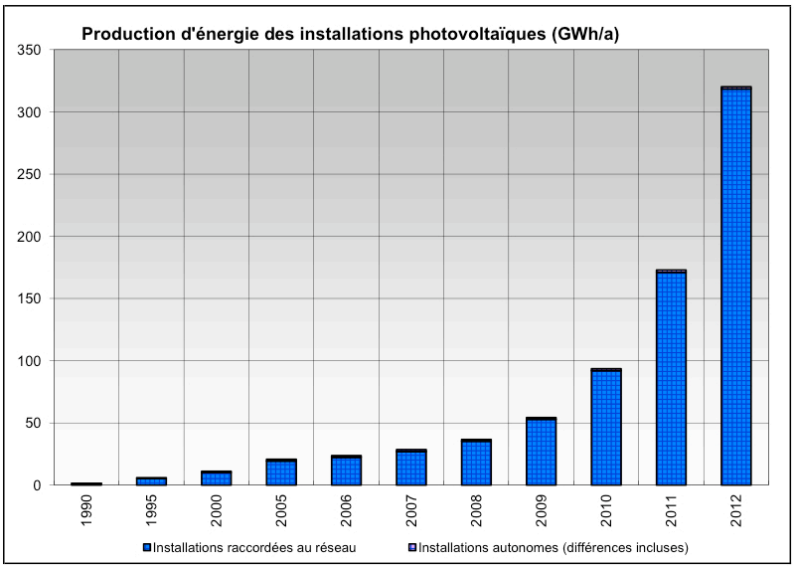

b) Energy production

Figure 1: Sales of solar modules on the left and produced energy on the right in Switzerland from 1990 until 2012 [SFOE, 2013]

Solar energy can be used in different forms: Mainly, by thermal collectors and by photovoltaic modules. Materials used as absorber layers for photovoltaic energy conversion include mono- and multi-crystalline silicon, amorphous and microcrystalline silicon, copper indium diselenide (CIS), dye-sensitized or organic materials. Previously achieved efficiencies and predictions for the next 120 years for different technologies are reported in [Goetzberger, 2002].

Silicon is the second most abundant material in the Earth, and can be directly used in gas state for thin-film solar cell technology. On the other hand, for crystalline solar cells it needs to be processed to be very pure before solar cell production.

The first amorphous silicon solar cell was developed in 1976 and the maximum efficiency that can be obtained was estimated to 14-15% [Carlson 1976]. Recently, the record efficiency at stabilized conditions reached 10.11% measured by National Institute of Advanced Industrial Science and Technology (AIST), Japan, 2013.

Main advantage of thin-film silicon technology consists in its reduced fabrication cost thanks to low-temperature deposition of thin layers on a substrate and its potential to large-scale application. Their efficiency is limited to a large extent by the charge collection due to poor absorber layer quality. This limits maximum thickness. To absorb still enough light, for thin-film silicon a-Si solar cells sophisticated techniques are recalled, such as light-trapping or the deposition of multi-junction solar cells in order to benefit from a larger range of the solar spectrum.

Particularly, the improvement of the performance in amorphous silicon solar cells concerns the quality of thin layers by increasing the collection of photo-generated electrical charges. The latter can be done with high quality doped layers, but also high quality intrinsic layers and interfaces are needed especially at the front of the solar cell. There, p-doped window layers are of special importancefor the collection of photo-generated charges while minimizing the parasitic absorption of light.

The present project aims to test a new p-type dopant, trimethylgallium (TMGa), for its use in amorphous p-layers in amorphous silicon solar cells.

This is done by developing and characterizing several series of p-layers doped with TMGa and with the standard p-dopant, trimethylboron (TMB). Later, p-i-n solar cells are fabricated with p-layers deposited according to most of these series to test if they are suited as window layers.

2. Theory

In the following two sections, 2.1. and 2.2., thin-film silicon solar cells and amorphous silicon will be described. The motivation for replacing the p-layer doping element boron by gallium will be presented in section 2.3.

2.1. Thin-film silicon solar cells

Solar cells classically known as modules are fabricated from silicon wafers, which consist of crystalline silicon (c-Si) with a well-organized atomic structure. The incident light is absorbed in the semi-conductor material, and is directly converted into electric energy. By photovoltaic energy conversion, the absorption of photons in the solar cell generates free electron and hole pairs. These photo-generated free charges are separated form each other thanks to the internal electric field created by the diode form of the solar cell. For c-Si, as a p-n junction, the internal electric field is limited in the depletion zone and the transport of carriers is by diffusion of free holes from n- and to p- side and of free electrons in opposite direction.

In thin-film silicon technology, however, amorphous or microcrystalline materials are used as absorber layers. Because of the disorder in the atomic structure, unwanted recombination of the charge carriers is enhanced as compared to crystalline silicon. Therefore, the electric field is extended over a larger zone by inserting a non-doped intrinsic absorber layer (i-) between p-and n-doped layers, as can be seen in figure 2 showing the band diagram of a p-i-n solar cell (right) in comparison with a p-n c-Si cell's band diagram (left). Thus, free charges are transported thanks to the extended internal elecrtic field by drift.

In both diode forms, negatively charged acceptors and positively charged donors form space charge regions, in p- and n- doped layers next to the interfaces with the intrinsic layer. The potential difference between these two regions in doped layers, defined as the built-in voltage (V_{bi}~1V), leads to the internal electric field from n- to p- doped side.

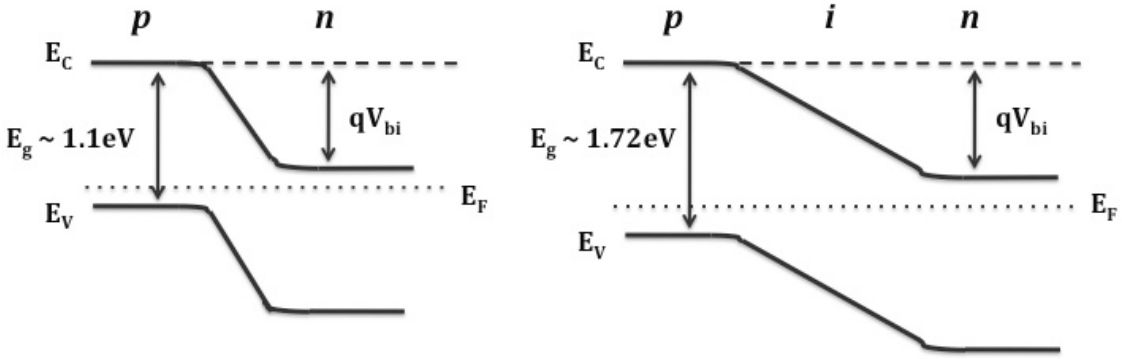

Figure 2: Band diagram of a p-n junction on the left and a p-i-n junction on the right

Amorphous silicon (a-Si:H) solar cells exist in two types, p-i-n and n-i-p, corresponding to the deposition sequence as illustrated in figure 3. The stacks of p-i-n and n-i-p layers are sandwiched between two transparent conductive oxide (TCO) layers. They do not only act as the electrical contacts but also as light scattering and transparent window layers thanks to their surface roughness as seen in the illustration below. As both, p-i-n and n-i-p type solar cells need to be illuminated through the p-layer, n-i-p cells can be deposited on opaque substrates such as metals or polymers.

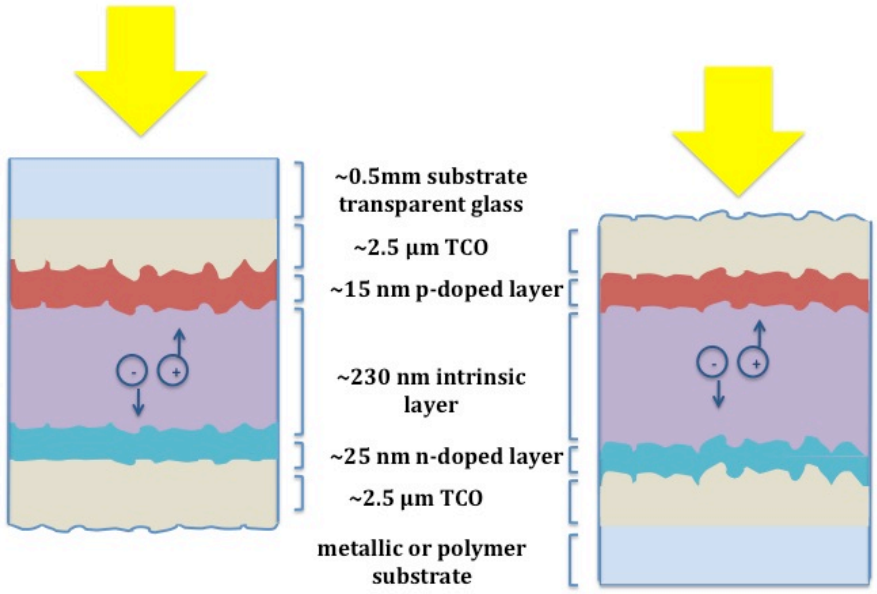

Figure 3: Amorphous silicon solar cells in p-i-n, on the left, and n-i-p, on the right, configurations

Silicon has an indirect band gap, which means that a phonon emission is required in order to absorb a photon creating a free electron and hole pair, because the maximum of the valence band and the minimum of the conduction band do not match in k-space. On the other hand, semiconductors presenting a direct band gap, which leads to a direct absorption of the photon only with the condition that its energy is larger than the energy band gap between the maximum if the valence band and the minimum of the conduction band. Thus, the absorption coefficient of these semiconductors with direct band gap is higher than the ones with indirect band gap. The absorption coefficient of amorphous silicon in visible light is between the one of direct and indirect band gap materials because of its non-direct band gap, see figure 4. Therefore, amorphous silicon can be used in thinner devices; hence, its production is possible with less material consumption. Nevertheless, light-trapping techniques are required for thin-film silicon devices, such that the absorber layer thickness can be kept small. In the present case, highly scattering front and back TCO layers and a scattering back reflector serve for light-trapping, enhancing the optical path and increasing the absorption in the intrinsic layer by multiple reflections. At the same time, it is important to reduce parasitic absorption in other layers than the intrinsic layer, which is typically done by keeping them thin and choosing materials with a wide energy band gap.

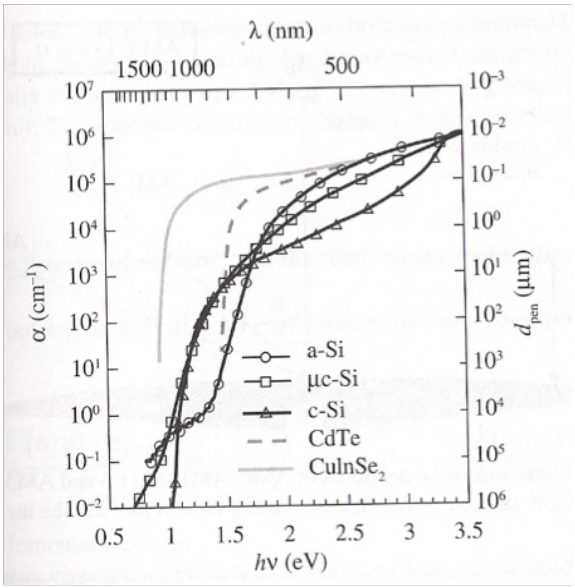

Figure 4: Absorption coefficient versus photon's incident for amorphous, microcrystalline, crystalline, CdTe and $CuInSe_2$ [Shah, 2010]

As an alternative technique to increase the performance of thin-film solar cells, two or more solar cells can be deposited successively forming multi-junction devices. Tandem cells, the goal being to benefit more from the solar spectrum, have two or more absorber materials with different band gap energies. Today's most important application of amorphous silicon solar cells is its implementation as top cell in a tandem device with a microcrystalline (µc-Si:H) bottom cell, a so-called micromorph solar cell developped by [Meier, 1994]. Top cell, with wide band gap, absorbs photons with higher energy than the remaining ones absorbed in the bottom cell.

2.1.1. Charge collection

Thanks to the internal electric field within the solar cell, photo-generated electron-hole pairs are separated and transported by drift until the contact layers to be collected. This type of transport is governed by the drift length of free electrons and holes. It should be larger than the i-layer thickness to guarantee the collection of free charges. As expressed in the equation (1), l_{drift} depends on the strength of the internal electric field (E) and on the quality of the intrinsic layer characterized by the mobility-lifetime product $\mu^0 \times \tau^0$ [Okamoto, 1982], where μ^0 is the band mobility of free charges and τ^0 the capture time by a defect in the i-layer.

$$l_{drift} = (\mu^0 \times \tau^0)\, E \qquad (1)$$

Impurities in the intrinsic layer increase the amount of the defects – typically in the form of dangling bonds –, which act as recombination centres. This reduces the fraction of the photo-generated electron-hole pairs that reaches the electrical contacts. With the rising number of dangling bonds acting as recombination centres, free carriers' time to be captured by one of them in the intrinsic layer is decreased, thus, the drift length. That is why the intrinsic layer needs special attention.

In doped layers, the defect density is dramatically higher as compared to intrinsic layers. Therefore, most electron-hole pairs recombine there directly after being photo-generated. Hence, the absorption of the light in the intrinsic layer primarily contributes to the photo-generated current and the thickness of doped layers must be kept as thin as possible to reduce this parasitic absorption. On the other hand, the primary role of the p- and n- doped layers is to assure the internal electric field through the intrinsic layer, which depends on the built-in voltage (V_{bi}) of the solar cell. The latter is the potential difference between the two doped layers and depends on the shift of Fermi level in the layers, thus, on the doping level of the layers. To provide a sufficiently high V_{bi} to create the internal electric field, a minimum thickness of doped layers with an appropriate doping level is required. Therefore, the best thickness for doped layers is a trade-off between maximizing electrical properties and minimizing optical absorption. In this study, to accentuate the effects of the new dopant, thicknesses of p-doped layers in p-i-n amorphous silicon solar cells were kept relatively high (~20 nm).

Nevertheless, minimizing the light absorption is very important for p-doped window layer of the solar cell. To minimize the absorption in the blue region of the light spectrum in particular and to increase V_{bi}, the band gap energy of the window layer needs to be increased. For this purpose, carbon – and oxygen – alloys, such as methane (CH_4) or carbon dioxide (CO_2), can be used during the plasma deposition [Tawada, 1981]. The carbon clusters settled in the amorphous silicon network form graphite-like very ordered clusters leading to the expansion of the band gap, which, on the other hand, reduces the conductivity of the films.

2.1.2. Electrical description of a-Si:H solar cells

Conversion efficiency (η) of a solar cell is expressed by the ratio of the maximum power of the solar cell to the power of the incident irradiance as described in equation (2). Thus, it depends not only on the performance of the cell but on the solar spectrum as well.

$$\eta = \frac{P_{max}}{P_{sun}} \tag{2}$$

In the dark, an a-Si:H solar cell can be described as a diode. Thus, the current density in the dark (J_{diode}) is expressed by an exponential function of the applied voltage (V) as described by equation (3), similarly to c-Si solar cells. J_0 is the dark saturation current density, q the elementary charge (1.6×10^{-19} C), k the Boltzmann's constant (1.38×10^{-23} J/K) and T is the temperature. The ideality factor (n) varies, usually, between 1.5 and 2. It describes the similarity of the diode to an ideal diode, and when increasing reduces J_{diode}.

$$J_{diode} = J_0 \left[exp\left(\frac{qV}{nkT}\right) - 1 \right] \tag{3}$$

However, when the a-Si:H solar cell is illuminated, the movement of photo-generated free charges will lead to a photo-generated current density (J_{photo}). Current density collected from the solar cell under illumination ($J_{illuminated}$) depends not only on the diode behaviour but also on losses by recombination ($J_{recombination}$) or in parallel resistance ($J_{parallel}$), as expressed in equation (4). This behaviour of an a-Si:H solar cell under illumination can be described with the equivalent electric circuit as drawn in figure 5.

$$J_{illuminated} = -J_{photo} + J_{recombination} + J_{diode} + J_{parallel} \tag{4}$$

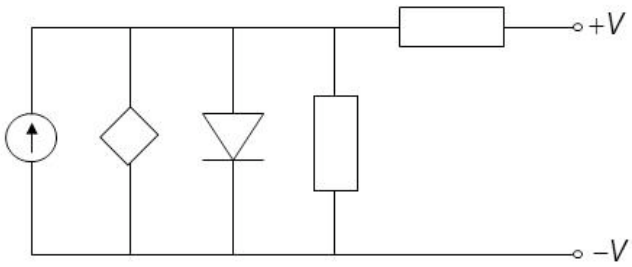

Figure 5: Equivalent electric circuit of a p-i-n solar cell representing from left to right: Photo-generated current density (J_{ph}), current density due to recombination losses (J_{rec}), diode with J_{diode} and resistance in parallel and in series with diode (schema by Michael Stuckelberger)

Series resistance (R_{series}) and parallel resistance ($R_{parallel}$) represent contact resistivity and ohmic shunts through the diode, respectively. Particles or impurities settled on the substrate or on the front TCO layer will cause a very low $R_{parallel}$, which will reduce the fill factor (FF) and the efficiency of the solar cell. On the other hand, R_{series} increases due to poor TCO properties or too resistive p- and n- layers.

Doped layers that are not thick enough or are insufficiently doped to create a strong internal electric field strong limit the separation of free holes and electrons. Hence, the open circuit voltage (V_{OC}) is reduced.

2.2. Amorphous silicon and doping

As mentioned before, the irregularities or defects in the atomic structure of amorphous silicon lead to a high density of electronic states in the middle of the band gap as well as at the band edges. The mid-gap states correspond to dangling bonds (DB) that are unsaturated bonds of silicon atoms and act as recombination centres. DB can be passivated by hydrogen (H) atoms that form Si-H bonds. Still, unpassivated dangling bonds can be found in the a-Si:H layers, which can, also, be passivated by an annealing treatment. However, higher deposition temperature of the intrinsic layer can help to anneal a part of DB already during deposition. On the other hand, the i-layer deposition temperature is limited because of possible etching of atoms from previously deposited layers, which will be re-deposited during the on-going deposition, and become impurities within the next layer. This is particularly important for the p-/i- interface that needs to be especially defect-free. Notably, the density of recombination centres within the a-Si:H increases under illumination until stabilizing asymptotically. This light-induced degradation, called Staebler-Wronski effect, is due to the weak bonds of the amorphous material, which break, even easier with higher light intensity, and create new dangling bonds. Light induced degradation due to Staebler-Wronski effect is reversible; the light-induced defects can be annealed out [Staebler and Wronski, 1977]. Higher annealing temperature induces a higher annealing rate. Another way to reduce the light induced degradation is to dilute silane (SiH_4) gas with hydrogen (H_2) during the plasma deposition. In fact, most stable materials are typically obtained under deposition conditions that are close to the transition to microcrystalline silicon, which depends on the hydrogen dilution of silane used in layer deposition as stated in [Keppner, 1999].

Conduction and valence band of a-Si:H is given by Fermi-Dirac function. The electronic states close to the edges of the conduction band (CB) and the valence band (VB) (more pronounced than CB) correspond to stretched and compressed Si-Si bonds. The density of states in the band tails decreases exponentially towards the middle of the band gap as showed in figure 6. These states, in their turn, act as trapping centres that will capture free carriers (electrons and holes) and re-emit them by thermal emission to the band from where it was captured (CB and VB, respectively). Trapped charges in the band tails of doped layers can lead to a deformation of the internal electric field, thus, to a reduction of charge collection [Stuckelberger, 2011].

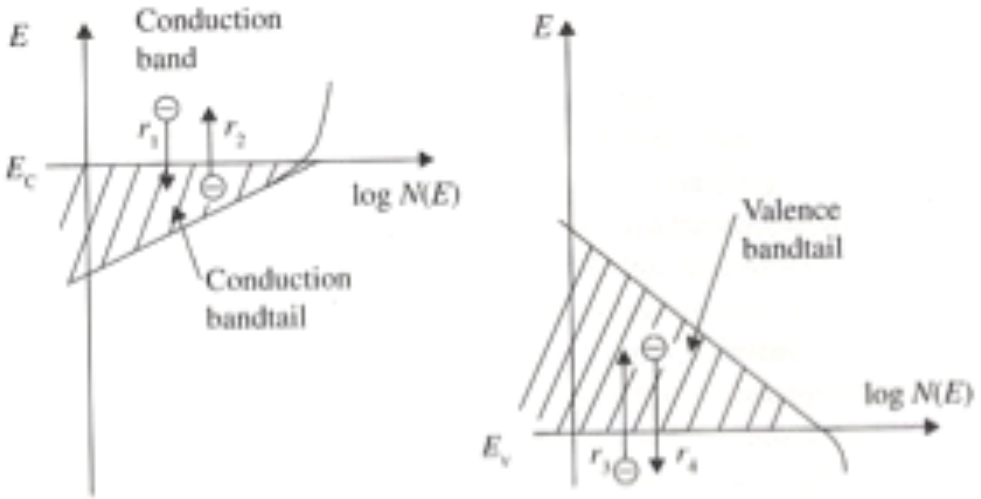

Figure 6: Conduction and valence band tails and exchange between free carriers from conduction and valence band and trapped carriers from corresponding band tail. [Shah, 2010]

The a-Si:H can be doped by introducing acceptors (p-dopants), or donors (n-dopants). Spear and Le Comber [Spear, 1975] showed that adding diborone (B_2H_6) or phosphine (PH_3) gases in the silane – hydrogen gas mixture during the plasma deposition resulted in p- and n-doped a-Si:H layers, respectively. Subsequently, Tarui, et al. demonstrated [Tarui, 1989] that using trimethylboron ($B(CH_3)_3$, TMB) instead of diborone as p-dopant resulted in a better doping efficiency with a lower density of band tail states. The band gap of p-layers with TMB is, as shown in the same article, wider than with diborane, which reduces parasitic absorption in the front layer particularly for short wavelengths. By doping, the Fermi level (E_F) shifts from mid-gap to the VB and CB for p- and n- doped layers, respectively. However, due to the band tail states, the shift is limited to ~0.2 eV away from the bands. Also, by greater amount of dopant in the layer the conductivity in the dark (σ_{dark}) of a-Si:H layers is increased until it saturates at ten times higher values with n-doped a-Si:H than with p-doped, as reported in [Spear, 1975]. σ_{dark} varies with the temperature (T) following equation (5), where the activation energy (E_{act}) can be used to determine E_F of the layer as the difference of energy needed, respectively, by a hole or an electron to reach the VB or the CB. An efficient doping, depending on the amount of acceptor or donors, would lower the activation energy and, consequently, increase the conductivity, which will also decrease the R_{series}.

$$\sigma_{dark} = \sigma_0 exp\left(\frac{-E_{act}}{kT}\right) \tag{5}$$

2.3. Boron-tailing

As the defect concentration in the absorber layer in a-Si:H solar cells needs be as small as possible, its deposition is processed with great caution, preferably in a separate chamber dedicated for intrinsic layers.

It is also recognized that increasing the deposition temperature of the i-layer results in reduction of the EQE at short wavelengths. If a negative bias voltage (V_{bias}) is applied on the electrical contacts of the solar cell, most of the EQE losses at short wavelengths caused by increased deposition temperature, recovers. Figure 7 shows EQE results, obtained by Michael Stuckelberger, of two p-i-n solar cells with i-layers deposited at 200 °C and at 250 °C, and present additional to the effects on the short wavelengths, a shift of the curves to the higher wavelengths. The latter is due to the decrease of the band gap when the deposition temperature is increased.

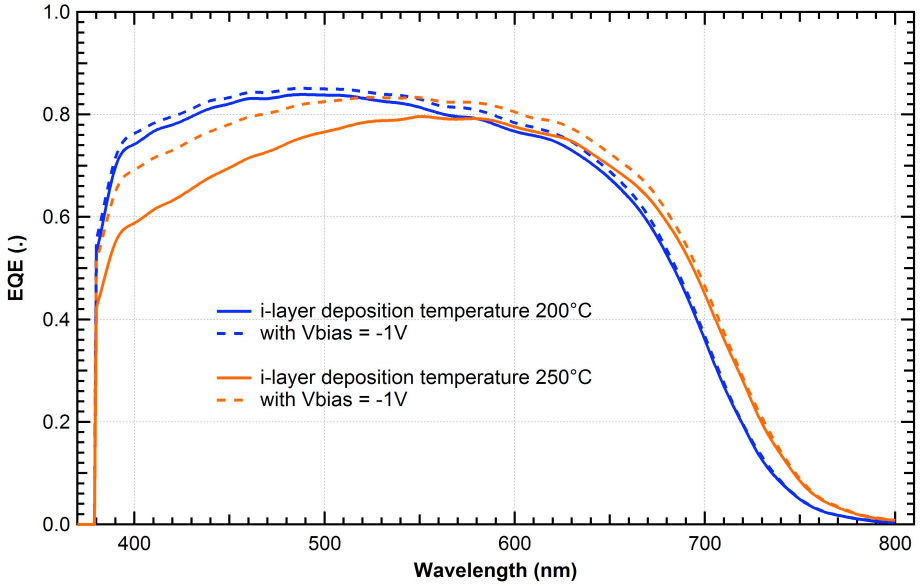

Figure 7: External quantum efficiency curves of two p-i-n solar cells with i-layers deposited at 200°C and at 250 °C.

EQE losses at short wavelengths are typically due to collection problems at the p-/i- interface. The reason of the observed recovery of these losses in the presence of V_{bias} is not completely clear. Though, one of the possible explanations is considered as an etching of boron atoms in the glow discharge of i-layer deposition at high temperatures. In fact, more agitated plasma in high temperatures could remove some of the previously deposited p-layer. Liberated boron atoms will eventully be re-deposited within the on-going i-layer deposition and become defects near the p-/i- interface, so-called boron-tailing effect.

Particularly for p-i-n solar cells, it is important to prevent the boron-tailing for a satisfying conversion of the incident photons in the absorber layer at short wavelengths. Thus, in this report, a new type p-dopant, trimethylgallium (TMGa), will be tested to replace possibly TMB.

3. Experimental details

Methods and systems used for the preparation and the characterization of the samples are specified in the first and second part of this chapter, respectively.

3.1. Processing steps

In this section, every stage of a thin-film solar cell deposition as well as a layer deposition performed during this project is explained in details. All depositions were made on Schott AF32 glass substrates. 8.2x4.1 cm^2 sized and 0.5 mm thick glasses.

3.1.1. Front and back contacts: transparent conductive oxide (TCO)

For front and back contacts, boron doped zinc oxide (ZnO:B) was used, obtained by low-pressure chemical vapour deposition (LPCVD) [Ding, 2013]. Both layers were deposited using the same recipe providing 2.5 µm thick ZnO:B, but the front contacts were deposited in the large XL system, the back contacts in the smaller chamber B.

The roughness of front contacts, beneficial for light scattering but limiting electrical performance of the cells, was reduced by an argon plasma treatment; the longer the plasma is on, the smoother the texture will be.

All cells were deposited during this project on four different substrates. Three of them were 2.5 µm thick ZnO:B; two of the three were exposed to an argon plasma during 7 and 20 minutes, respectively. The fourth substrate was either smoothly grown LPCVD ZnO (4 minutes argon plasma treated) or a glass substrate.

3.1.2. Plasma enhanced chemical vapour deposition (PECVD)

All layers as well as the cells were fabricated by plasma enhanced chemical vapour deposition (PECVD), which results in low defect density in the deposited a-Si:H layer as compared to other techniques such as sputtering and evaporation of the pure silicon [Chittick, 1969].

In PECVD, a gas mixture, consisting principally of silane (SiH_4), is injected in the deposition chamber at certain ratios according to the wanted layer characteristics. Gas flows are expressed by standard cubic centimetre per minute (sccm). The substrate, kept in a holder, is placed between two electrodes, one connected to the ground charge while the other will be encountered with an electrical power. The electrode containing the substrate holder is particularly assigned to heat the substrate before the deposition starts. As the plasma is ignited, the present gas molecules are ionized. Radicals and ions, reacting with the atoms on the surfaces exposed to the plasma, will stick on them and constitute an element of the deposited layer. The growth of the latter depends strongly on the deposition parameters such as the pressure, the substrate temperature, the frequency, the net power in the plasma and obviously the amount of the inserted gases.

System B installed in the grey room of PV-Lab, Neuchâtel, was used for PECVD processes within this project. It is a manual system, meaning that every step mentioned above is performed manually, and consists of two vacuumed deposition chambers and one load-lock. One of the chambers is used only for doped layer deposition and the other only for intrinsic layer deposition in order to minimize the contamination in the i-layer. Different gases are connected to the system B through the corresponding mass flow controller (MFC); two for pure SiH_4 limited to 10 and 100 sccm, for TMB two sources are available one diluted at 2% in H_2 and the other at 500 ppm in H_2, as n-dopant one with PH_3 0.1 % diluted in H_2 is limited to 100 sccm, for carbide and hydrogen contents one with pure CH_4 and one with pure CO_2, both limited to 10 sccm, for pure H_2 one MFC is used limited to 100 sccm. Finally, pure gallium (Ga) dopant in form of TMGa is connected to the system. Its MFC requires at least 0.2 sccm to get a stable gas flow. The pressure is controlled by a butterfly valve between the

chamber and the pumping unit, either according to its position or the wanted deposition pressure. The excitation frequency is set by a frequency generator, and the power amplification is adjusted with the help of a directional powermeter. The substrate temperature is controlled via the electrode plates, for this purpose there four temperature controllers are connected for both electrodes; two in both chambers.

For layer series in this project, one deposition parameter was varied for each series. For solar cells a baseline p-i-n solar cell recipe, corresponding to a cell design shown in figure 8, was used varying only one of the a-Si:H p-layer parameters for each series. Doped µc-Si layers were inserted between doped a-Si:H and TCO layers to enhance the transport of free charges at critical interfaces. Additionally, a carbon dioxide plasma treatment was performed before both µc-Si layers in order to facilitate the µc-Si growth. The intrinsic layer is deposited progressively; firstly a a-SiC:H buffer layer with a high hydrogen dilution is fabricated and secondly the a-Si:H active absorber layer is deposited. Hydrogen dilution in PECVD is known to increase the band gap and thereby also the absorption in short wavelengths and the open circuit voltage. Therefore, the buffer layer was inserted in the first part of the deposition.

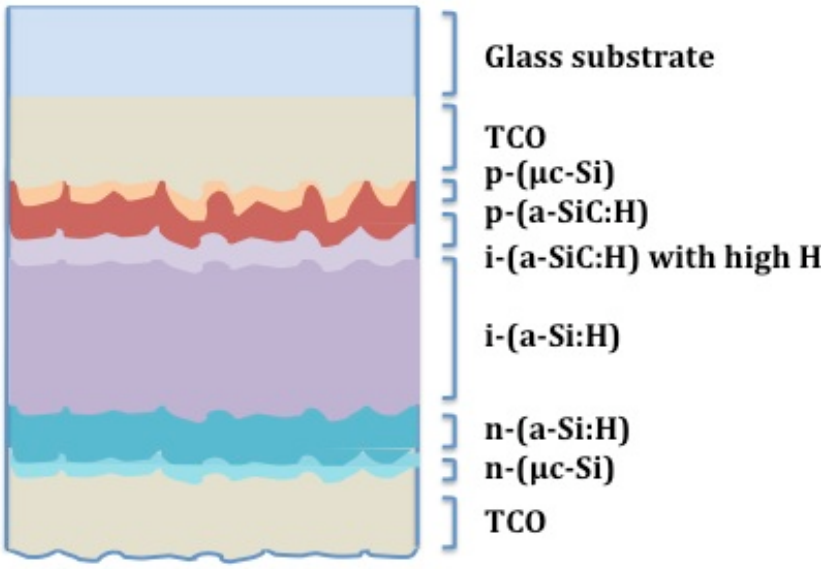

Figure 8: Cell desgin of standard p-i-n a-Si:H solar cell for system B.

3.1.3. Structuring of the cells

After all cell deposition processes, detailed in sections 3.1.1. and 3.1.2., are completed, the 4x4cm^2 glass substrate forms only one single thin-film silicon solar cell. In this state, a lift-off mask was used and an organic felt pen to cover some parts of the surface in order to define 16 seperate 0.25x0.25cm^2 sized cells. Only then, the back contact layer was deposited, from which the parts containing the ink underneath are removed in an acetone bath.

To get access to the front contact layer of the solar cells, the silicon layers between the cells were subsequently etched by sulphur hexafluoride (SF6) plasma.

3.2. Layer characterization

Measurement tools with their principles and the characterization methods used during this project to determine electrical and optical properties of p-layers are described in the following sections.

3.2.1. Dark conductivity measurements

At first, two 100 nm thick aluminium contacts with 0.5 mm distance in between are deposited on the layer by thermal evaporation. The aluminium (Al) is heated by the current crossing the tungsten boat holding the Al sticks and is evaporated at 10^{-5} mbar in the deposition chamber.

The conductivity (σ) of the deposited layer can be determined by the measurement of the generated current due to the electric field (E) that exists between two metallic contacts at a distance (l) where a voltage (V) is applied. The current density (J), assumed to be uniform in the cross section, is expressed in terms of the electric field and conductivity as shown in equation (6).

$$J = \sigma E = \sigma \frac{V}{l} \tag{6}$$

To determine temperature dependant σ_{dark} and the E_{act} of the layers, the current was measured in a dark chamber with a pressure around 10^{-1} mbar while the temperature rises up to 180 °C in 15 minutes, stays constant during 1.5 hours, and decreases then to room temperaturein 2.5 hours and stays for 2 more hours. The real temperature in the dark chamber follows this regulation, however, a delay is observed decreasing the temperature due to a lack of active cooling. When σ_{dark}, expressed as in equation (5), is plotted in an Arrhenius plot, according to the equation (7) for p-doped layers, the corresponding activation energy can be deducted from the slope of the decreasing conductivity.

$$\ln(\sigma_{dark}) \approx ln(\sigma_0) - \frac{(E_F - E_V)}{kT} \tag{7}$$

As compared to equation (5), $(E_F - E_V)$ represents here the activation energy, as the valence band tail is dominant. For n-type layers the activation energy is expressed with $(E_C - E_F)$. In this project, every Arrhenius plot obtained with p-doped layers was linearly fitted in order to determine the slope at decreasing temperature in the range of ~180 °C to 100 °C.

3.2.2. Photospectrometry

A Lambda 900 spectrometer from Perkin Elmer was used for transmission measurements of the deposited layers. A monochromatic light beam with a wavelength between 320 and 2000 nm hits the sample where it is transmitted into an integrating sphere.

This measurement is performed particularly to enhance the reliability of the results from the ellipsometry analysis.

3.2.3. Ellipsometry

The ellipsometer used for the characterization of the layers is a UVISEL ellipsometer from Horiba Jobin Yvon including monochromators for the infrared (IR) and for the ultraviolet/visible (UV/VIS) parts of the spectrum. The sample is placed in the middle of the holder and illuminated with an elliptically polarized light. The beam is reflected with the same incidence angle and is detected in the monochromators between 0.6 eV to 6 eV to deduce the variance of the polarization, quantified by the phase difference and the intensity ratio between the incident and the reflected light. For this project, each layer was measured at three angles 50°, 60° and 70°, 0° being perpendicular to the sample's surface.

This indirect method is based on varying the parameters in an iterative way from an assumption until obtaining the best fit to the measurement. That is why optical models are needed for the layers under investigation.

The analysis of the measurements was performed by Michael Stuckelberger with Tauc-Lorentz oscillators in order to determine the thickness and the band gap energy of the layers.

3.3. Solar cell characterization

In the following sections two principal techniques to measure the performance of the deposited solar cells are reported.

3.3.1. Current – voltage measurements

A four-lamp (three halogen lamps, one xenon lamp) solar simulator from Wacom was used under standard test conditions (AM1.5g, 1000 Wm^{-2}, at 25 °C) to measure the current - voltage characteristics from -1 to 1 V. The substrates were placed on a block where two pairs of pins are connected, each for measuring the current and the voltage independently. A ventilator is used to cool the cells. Every sample was measured once under full illumination and once in the presence of a filter blocking 99.6% of the incident light. From the J(V) curve in particular the fill factor (FF) of the cell can be calculated, which represents the ratio of its maximum power point (MPP) to the product V_{OC} x J_{SC}, as expressed in equation (8).

$$FF = \frac{P_{max}}{(V_{OC}\, J_{SC})} = \frac{(V_{max}\, I_{max})}{(V_{OC}\, J_{SC})} \qquad (8)$$

The open circuit voltage (V_{OC}) is the electric tension between the two electrodes when no current crossing the illuminated cell, and can be determined from the J(V) curve. V_{OC}, depending on the diode behaviour of the solar cell, is theoretically and practically limited at a maximum value depending on the band gap of the material. The short circuit current density (J_{SC}) is obtained while the voltage at two contacts is equal to zero and depends directly on the number of photo-generated free electrons and holes, thereby on the band gap, absorption coefficient and the thickness of the device.

Actually in the PECVD system used for this project the deposition is not completely homogeneous on the substrate's surface. For this reason, for all measurements we focused our attention to the centre of the samples. So for the external quantum efficiency measurements the cell with the highest FF x V_{OC} product among the 4 central ones was chosen. As the area of the cells prepared for this project is not defined that precisely the current density obtained here were not significantly taken into consideration.

3.3.2. External quantum efficiency measurements

The ratio of the collected electrical charges to the incident photons is the external quantum efficiency (EQE) of the solar cell. EQE curve plotted versus the wavelength of the incident light gives indications about the losses due to the reflection and absorption in doped layers. As short-wavelength photons with higher energies are absorbed mostly in the front of the solar cell, smaller EQE values will represent the losses at the front. Similarly, penetrating until the back of the solar cell, the long wavelengths may be lost by parasitic absorption if the back reflector does not assist a fine light scattering back in the absorber i-layer or if back TCO layer is not enough transparent.

EQE curves were measured, using a homemade tool, relative to a reference cell integrated in the system. A xenon lamp, with a varying wavelength between 370 and 810 nm with an increment of 10 nm, is directed to a chopper for lock-in measurement. After a beam splitter one part reaches the reference cell, while the other part is focused to the centre of the probed cell. In order to simulate operational conditions similar to the standard test conditions the cell is also illuminated by an external bias light composed of 4 white LEDs. The

sample is fixed on the holder plate with a white reflector stuck behind the measured cell. A couple of pins connected to the two electrodes from the back of the solar cell detect the current generated under illumination. Subsequently, measurements under an additional bias voltage of -1 V were also performed to identify collection problems within the device. Lastly, the short circuit current of the cell was deducted during this project by integrating the EQE curve over solar spectrum ($\Phi_{AM1.5}(\lambda)$) folowing equation (9).

$$J_{SC}(V_{bias}) = \int_{\lambda_{min}}^{\lambda_{max}} SR(V_{bias}, \lambda) \cdot \Phi_{AM1.5}(\lambda) \cdot d\lambda$$

$$\text{Where } SR(V_{bias}, \lambda) = EQE(V_{bias}, \lambda) \cdot \frac{q}{E(\lambda)} \tag{9}$$

4. Results and discussions

In purpose of comparing electrical and optical characteristics of amorphous silicon p-type layers with different dopants, gallium and boron, several series of layers were fabricated by PECVD. The most interesting series were than incorporated in amorphous silicon solar cells in p-i-n configuration, which were realized based on the standard cell. The latter's design is showed in section 3.1.2. and results are presented in the section 4.2. Layer and solar cell series will be discussed in the following sections of this chapter. More precisely, the varied deposition parameters of p-(a-Si(C):H) layers include:

- *Dopant flow*
- *Silane (SiH_4) flow*
- *Methane (CH_4) flow*
- *Power*
- *Temperature*
- *Layer thickness*

In a last series, the effect of i-layer deposition temperature on EQE was investigated with respect to boron or gallium tailing characteristics. Frequency used in plasma depositions was at 70 MHz for all doped layers.

Finally, the layers have electrically and optically been characterized in terms of activation energy (E_{act}) from dark conductivity measurements, and the Tauc-Lorentz energy band gap (E_{gap}) from ellipsometry measurements, as described in the previous chapter.

For the corresponding solar cells, the p-layers thickness was 20 nm according to the deposition rate determined from ellipsometry measurements. The performance of the solar cells is discussed particularly with respect to variations of the open circuit voltage (V_{OC}) and the external quantum efficiency (EQE). Results presented, herein this report, were determined for solar cell with front TCO layer that have been treated 7 minutes in argon plasma.

Experimentally, constraints were mainly given by the MFC of TMGa not allowing for lower flows than 0.2 sccm. As TMB was used as 2 % dilution in hydrogen, it was not in all cases possible to achieve the same deposition conditions for gallium and boron. Note, however, that all flow indications given in this report are real flows referring to pure gases. If nothing else is mentioned, the flow indications given in the graphs in the following sections refer to p-layer deposition conditions.

4.1. Reproducibility

In this section, we investigate the reproducibility of p-(a-SiC:H) layers. Over six months, five layers were deposited with the same deposition parameters. The reproducibility of the deposition process and of the layer characterization is discussed with respect to band gap and activation energy, which are shown in figure 9.

The band gap energy is 2.0 eV for this standard p-(a-SiC:H) layer deposited with 0.1 sccm TMB, 4 sccm SiH_4, 8 sccm H_2 and 8 sccm CH_4 at 5 W. It shows little variation of less then one percent among the five samples and lies within measurement error of ellipsometry.

The activation energy is around 0.5 eV, with a variation that is only slightly higher than for the band gap, if sample #4 is not taken in account. For this latter a big difference of 0.07 eV from the average is obtained in the activation energy. This may be due to an experimental inconvenience leading to a lower conductivity.

These results demonstrate that the layer depositions and measurement procedures are highly reproducible and variations well below observed effects that are reported in the following sections.

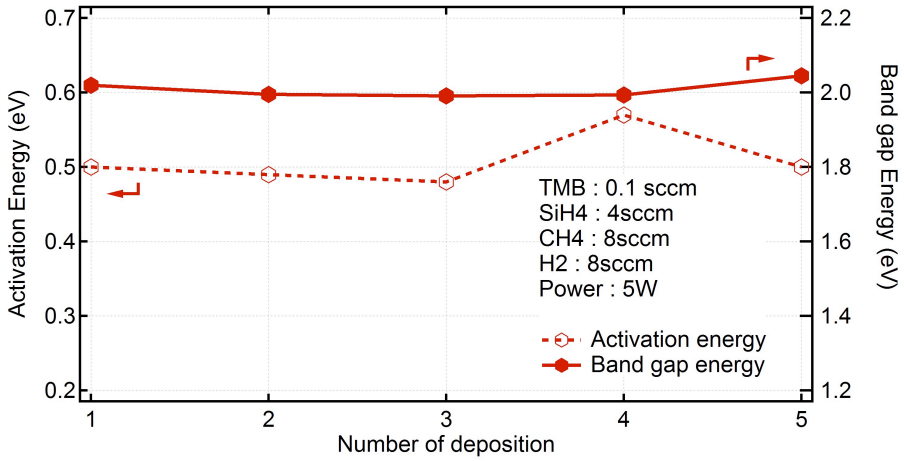

Figure 9: Band gap and activation energies for samples processed on different dates with the same deposition parameters.

4.2. Standard p-i-n amorphous silicon solar cell

For system B, a baseline cell recipe was developed at PV-Lab for p-i-n configuration and includes a p-layer deposited with a gas mixture of 0.1 sccm TMB, 4 sccm SiH_4, 8 sccm CH_4 and 8 sccm H_2 at 5 W and 200 °C during 10 seconds. To investigate the effects of p-layer thickness, the same solar cell recipe was deposited once as it is and secondly with a deposition process of 40 seconds for p-(a-SiC:H) layer. Characteristic values of two solar cells are reported in table 1.

Table 1: Efficiency, open circuit voltage, short circuit current density and fill factor values for standard p-i-n solar cell and standard p-i-n solar cell with thicker p-layer

	Efficiency	*V_{OC}*	*J_{SC}*	*Fill Factor*
Standard cell recipe	*11.66 %*	*900.4 mV*	*15.99 mA/cm^2*	*73.10*
Standard cell recipe with thicker p-layer	*9.41 %*	*926.74 mV*	*14.97 mA/cm^2*	*65.32*

For a p-i-n solar cell, thickening the p-layer decreases the portion of the light spectrum that reaches the absorber layer, especially for short wavelengths. Thus, less photo-generated electron-hole pairs are generated, which leads to lower current. However, increasing the p-layer thickness leads to a higher internal electric field, hence, increased V_{OC}.

The effect of increased thickness of the front layer in solar cells can be seen as a strong drop of the external quantum efficiency at short wavelengths, see figure 10.

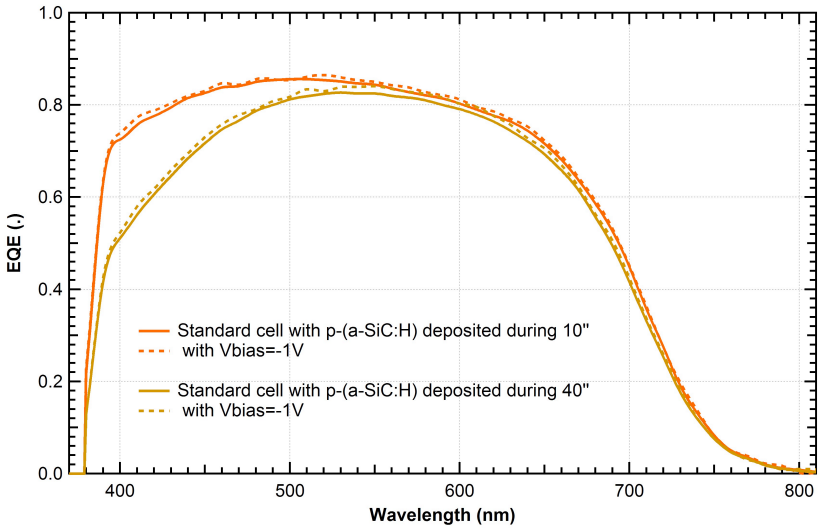

Figure 10: External quantum efficiency curves for standard p-i-n solar cell and standard p-i-n solar cell with thicker p-layer.

4.3. Power series of p-(a-SiC:H)

The effect of the power during the plasma process on p-layers containing gallium or boron dopant is studied in this section. With boron doping, a standard p-layer recipe was deposited using 0.1 sccm TMB, 4 sccm SiH_4, 8 sccm CH_4 and 12.9 sccm H_2, at varying the power. Though, due to the limitations mentioned earlier, TMGa gas was used at its minimum flow of 0.2 sccm with 10 sccm SiH_4, 10 sccm CH_4 and 100 sccm H_2. Preliminary tests with gallium showed better results of these gas flows as compared to the flow ratios used for depositions containing boron.

Figure 11 shows clearly that band gap and activation energies of the deposited layers change on the opposite directions if the plasma power in increased, both for gallium and boron doping. Wang and his group [Wang, 1999] have studied the effect of the plasma power on the series with varying CH_4 flow and concluded that at higher powers the carbon content in the layer is bonded with silicon atoms in favour of larger band gap. Similarly, a continuous increase of E_{gap} is observed with different base recipes for Ga and B.

Notably, varying deposition power impacts also the E_{act} of the deposited layers; when increased the dark conductivity activation energy is reduced in the same order of the band gap widening. Except at the point, where 10 W is applied a peak has been found in the activation energy of the layer containing B; this must be due to an experimental error.

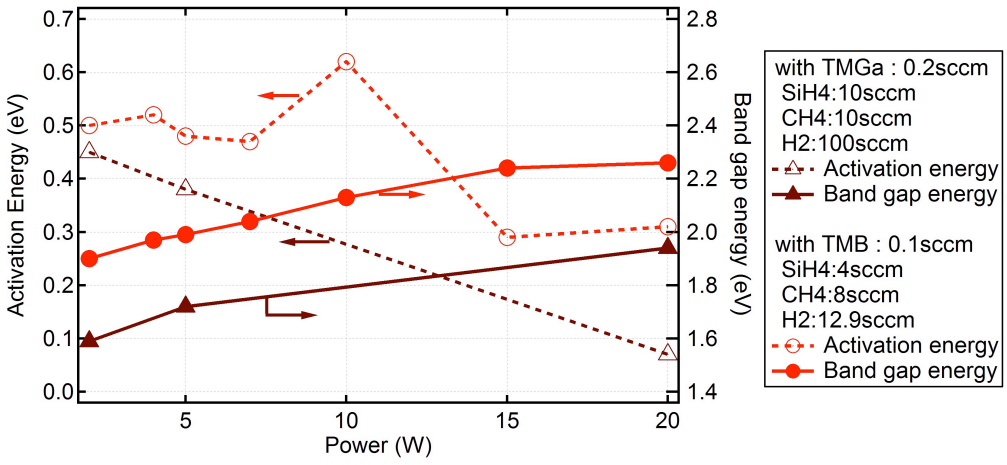

Figure 11: Band gap and activation energies of p-(a-SiC:H) layers doped by TMGa or TMB with varying deposition power.

Best electrical and optical parameters are obtained at the highest deposition power, 20 W. However, with that high power the deposition rate in PECVD is strongly increased, thus the reproducibility for such thin layers is poor. Besides, cells containing p-layers deposited previously at high power did not work. Possibly due to the increased ion bombardment during depositions at very high power, previously deposited ultra-thin p-(µc-Si:H) layer could be completely etched off the surface. That's why for succeeding depositions of all p-layers, alone or in a cell, 5 W was used.

4.4. Dopant flow series of p-(a-SiC:H)

In account of comparing the consequences of dopant amount (B or Ga) in the p-layers, the ratio of TMB and TMGa to the silane flow was varied in two series. Both were deposited with 8 sccm SiH_4, 10 sccm CH_4 and 25.8 sccm H_2 at 200 °C with 5 W. Because of the MFC limitations mentioned in section 3.1.2., the same range of the dopant flow ratios was not accessible. Thus, TMGa flow was varied between 0.2, 0.4, 0.8, 1.6 and 3.2 sccm, while TMB flow was varied between 0.05, 0.1, 0.2, and 0.4 sccm. For the highest boron concentrations of 10% TMB relative to SiH_4 flow, 0.4 sccm TMB and 4 sccm SiH_4 were used.

It is inevitable to notice in the figure 12, the same tendencies in changes of band gap and activation energies of the layer with the increasing correspondent doping gas flow, contrarily to the power series. In particular, layers containing Ga suffer much more from a band gap decrease with the increasing ratio of doping atoms than with B; Ga starts to infest the a-SiC:H layer after certain quantity instead of doping silicon. In this series, with more than 5% of TMGa in silane the E_{gap} becomes too narrow for doped a-SiC:H layers. In these cases, the Fermi level is observed to move towards the middle of the band gap, indicating reduced doping effect, and [Li, 1994] stated doping efficiency of Ga lower than B.

From process point of view, an intresting issue occurred for the sample with 40% of TMGa: it was not possible to fit the ellipsometry data with a simple Tauc-Lorentz model. Furthermore, several consecutive etching trials in SF6 plasma were not successful for this sample. Obviously, the layer must be composed of a different type of Si-Ga alloy rather than p-doped amourphous silicon and, if needed, requires further investigation to clarify it. These deposition conditions are not suitable for photovoltaic application but may be useful in other field. Clearly, lower TMGa ratios in silane need to be explored for eventual better characteristics concerning their implementation in window layers of p-i-n solar cells.

As for doping with TMB results in better quality window layers than TMGa thanks to higher E_{gap}. With higher TMB flow ratios, the band gap is narrowed in the range of 0.1 eV. A very similar trend in the same order of mangitude of the E_{gap} for B dopant amount in the deposition was reported in [Tarui, 1989] and [Lloret, 1992].

From the corresponding activation energies, the shift of Fermi level can be estimated to be smaller with low or with high TMB ratios in silane, and the lowest activation energy is obtained with 2.5% TMB in SiH_4. Hence, the optimum point for a wide band gap while keeping low the activation energy is acquired at 2.5% of TMB in silane with the values of E_{act} equal to 0.44 eV and E_{gap} to 1.85 eV.

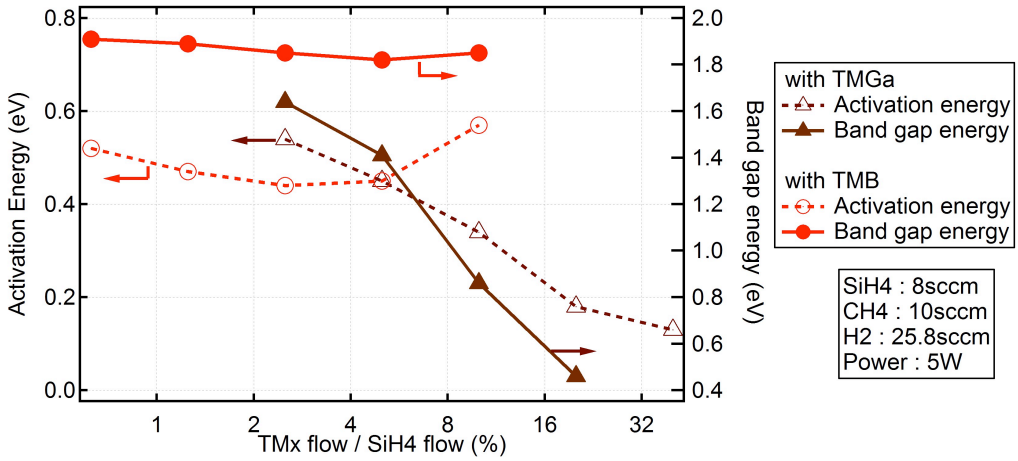

Figure 12: Band gap and activation energies of p-(a-SiC:H) layers doped by TMGa or TMB with varying doping flow ratio to silane.

As the thickness of all the samples could not be determined by ellipsometry analysis these layers were incorporated in p-i-n amorphous silicon solar cells with a deposition process time of 40 seconds, instead of the corresponding process time to a thickness of 20 nm.

A decrease in V_{OC} of slightly more than 20 mV in total is observed in figure 13 for solar cells containing p-layers with increasing TMB doping gas flow. This follows the trend of band gap narrowing and is probably due to more defects acting as recombination centres in the p-layer with the increasing doping level.

Obviously, low V_{OC} values for a p-i-n a-SiC:H solar cells have been obtained with p-layers deposited with high TMGa flows. However, lowering the Ga content in the p-layer leads to a strong increase of V_{OC}. For lower Ga contents than what is possible with current hardware, even higher V_{OC} values may be obtained.

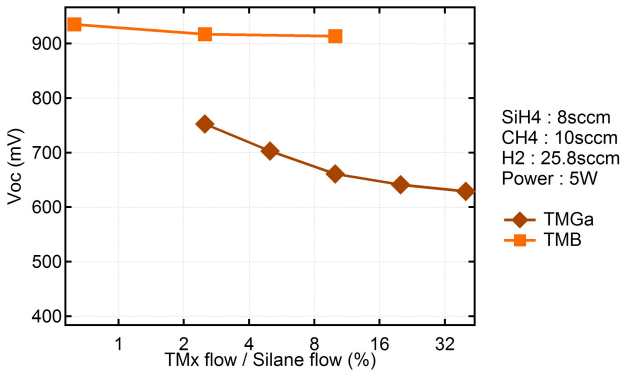

Figure 13: Open circuit voltages of p-i-n solar cells with p-(a-SiC:H) layers doped by TMGa or TMB with varying doping flow ratio to silane.

Increasing the flow ratio of TMGa to silane in the p-layers of solar cells results in a reduction of the EQE on the entire light spectrum as reported in figure 14 a). In fact, p-layers containing large Ga fractions absorbed a significant fraction of the incoming light.

On the other hand, increasing B contentin the p-layer of solar cells leads to a EQE decrease only for the blue region of the light, seen in figure 14 b). As expected from the band gap narrowing for p-layers containing high amounts of B dopant, when deposited in p-i-n solar cells these layers absorb short wavelengths of the light before it can reach the intrinsicabsorber layer. Yet EQE curves of solar cells with p-layers containing B are significantly higher than the ones containing Ga. Considering this and also the tendency to a more performing solar cells in lower ratios of TMGa to SiH_4, future studies on gallium should take in account lower TMGa flows.

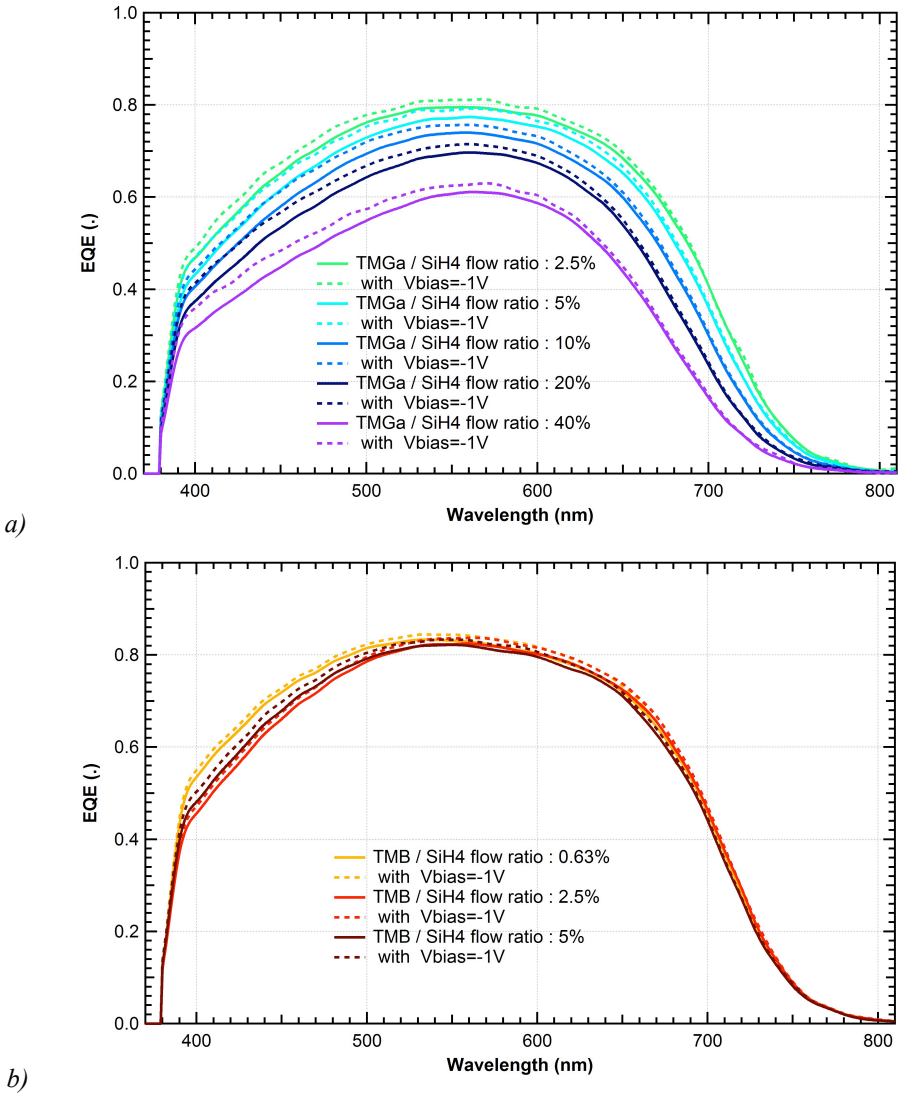

Figure 14: External quantum efficiency curves of p-i-n solar cells with p-(a-SiC:H) layers doped in a) by TMGa or in b) by TMB with varying doping flow ratio to silane.

Finally 0.2 sccm of dopant at 2.5% of SiH_4 in this series revealed for Ga the best p-layer characteristics. Therefore, further series of this project were produced with this ratio of gas flows.

4.5. Silane flow series of p-(a-Si:H)

Two series of p-(a-Si:H) layers have been deposited, without methane, using different quantities of silane in order to compare the characteristics obtained with Ga and B dopant. A H_2 flow of 100 sccm was used with 0.2 sccm of each doping gas for the layer depositions at 200 °C with 5 W. Different silane flows were 1, 2.5, 5, 10, 20, 40 and 80 sccm. Then, these p-layers were incorporated into p-i-n solar cells with silane flows of 1, 5, 20 and 80 sccm.

Band gap energy of boron doped layers increases notably with the introduction of more than 1 sccm SiH_4 and much less with higher silane flows until reaching a maximum level, as you can see in figure 15. As for Ga doped p-(a-Si:H) layers, similarly, increased silane flow leads to a wider band gap reaching almost the same level as B, although from much lower values. In fact, low silane amount in deposition of Ga doped p-layer results in a E_{gap}, again reaching almost 0.1 eV, which does not correspond to a band gap of amorphous silicon. Meanwhile, E_{act} for p-layers with B dopant increases slightly with higher silane flows. As for Ga-doped layers E_{act} follows mostly the changes of band gap staying close to $E_{gap}/2$. Hence,

the Fermi level for these layers is placed in the middle of the gap and only poorly shifted for all silane flows for a window layer with TMGa doping in p-i-n a-Si:H solar cell. Except with 20 sccm SiH_4 flow a much lower E_{act} is observed than the trend, and may be to a deposition problem. We can conclude that electrical properties of p-layers are slightly affected by different silane flows.

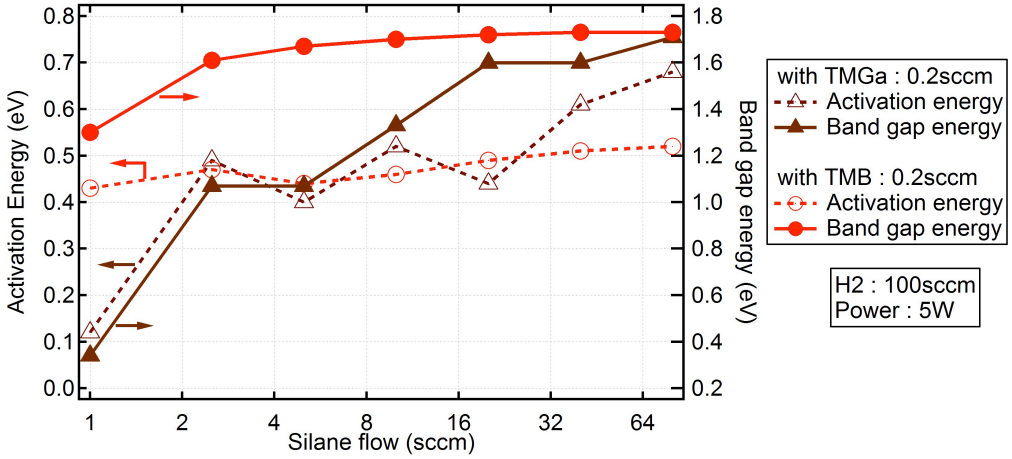

Figure 15: Band gap and activation energies of p-(a-Si:H) layers doped by Ga or B with varying SiH_4 flow.

The V_{OC} of solar cells containing a p-layer doped with TMB increases when the silane flow used for these layers is increased, as seen in figure 16. However, increase in the silane flow in the p-layer with TMGa doping in solar cells resulted first in an increase until the flow reaches 20 sccm, then in a great decrease of V_{OC}. The peak observed with Ga can be explained by the significant shift of the Fermi level leading to a stronger internal electric field transporting free charges to the both ends of the solar cell, which is reduced back again for even higher silane flow. This may be an interesting behaviour of gallium, as observed with two different layer depositions, though, needs further trials to assure that is not an error.

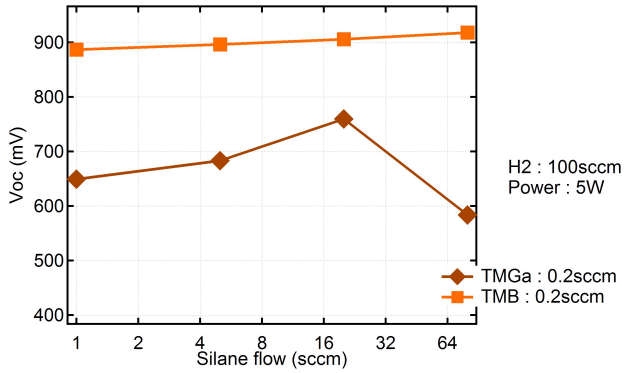

Figure 16: Open circuit voltages of p-i-n solar cells with p-(a-Si:H) layers doped by TMGa or TMB with varying SiH_4 flow.

EQE curves in figure 17 b) shows a clear increase of the parasitic absorption in the p-layer of the solar cells with boron doping, when the silane flow is increased. On the other hand, in solar cells with with gallium as dopant, displayed in figure 17 a), raised silane flow results in an increase at long wavelengths of the spectrum meaning that the absorption in the window layer is reduced. For short wavelengths, a reduction of EQE for 5 sccm SiH_4 in the p-layer is observed. This may be caused by an impurity interfered before or during the p-layer deposition preventing the penetration of the blue region into the absorber layer. Anyhow, the EQE of the solar cells containing Ga dopant in the p-layer is mostly lower than the ones with B dopant due to stronger parasitic absorption in the p-layer with gallium, as reported above. Additionally, with the solar cell containing Ga doped p-layer with 80 sccm SiH_4, if a

bias voltage of -1 V is applied, an increase of almost a factor of 1.5 is noticed in the same region of the light. That shows that the internal electric field is not strong enough to transport the charges until the electrical contacts if high silane flow is used for Ga doped p-layer doped, which was also observed with low V_{OC}.

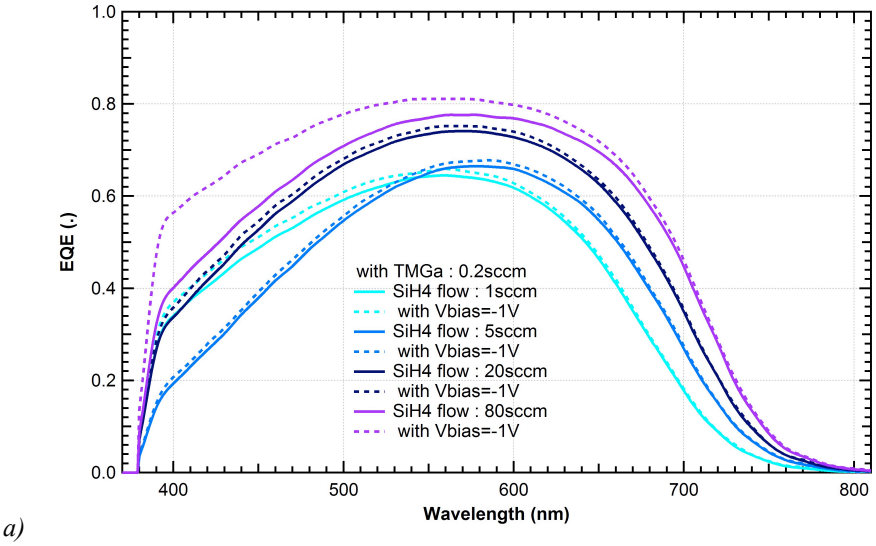

a)

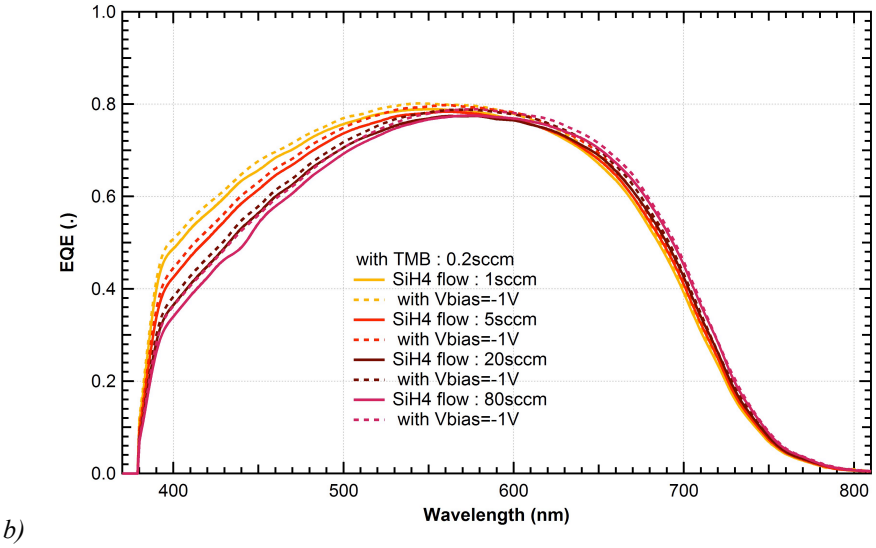

b)

Figure 17: External quantum efficiency curves of p-i-n solar cells with p-(a-Si:H) layers doped in a) by TMGa or in b) by TMB with varying SiH_4 flow.

4.6. Silane flow series of p-(a-SiC:H)

For this series of p-(a-SiC:H) layers, the same deposition conditions as in the previous section were used. However, 10 sccm of CH_4 is added this time.

As displayed in figure 18, increasing the silane flow for boron-doped hydrogenated silicon carbide layers leads to an increase in E_{gap} that reaches its maximum before saturating around 1.8 eV. With Ga dopant, the layers with lowest SiH_4 have again a very narrow band gap (below 0.1 eV), despite the presence of the carbon; silane flow was too low. However, it increases until reaching almost the same value as the layer containing B with, also, the highest silane flow.

The activation energy of the Ga doped film strongly increases with higher silane flows, whereas the silane-flow dependence is weaker with B doping. Theses changes of E_{act} lead to a shift of the Fermi level near $E_{gap}/2$ for layers containing B as dopant with the corresponding band gap energy when SiH_4 flow is increased. As for Ga doping in the a-SiC:H layers changes

observed resulted in a shift of the Fermi level away the mid gap, indicating that Ga dopant effect is more pronounced in a-SiC:H with a medium flow of SiH_4. Thus, they could assure high internal electric field if deposited in solar cell. Yet, activation energies are too high for concerned layers to be used in high performing p-i-n solar cells and band gap not wide enough, in fact maximum 1.72 eV gallium doping, which is still far below the gand gap of boron-doped layers.

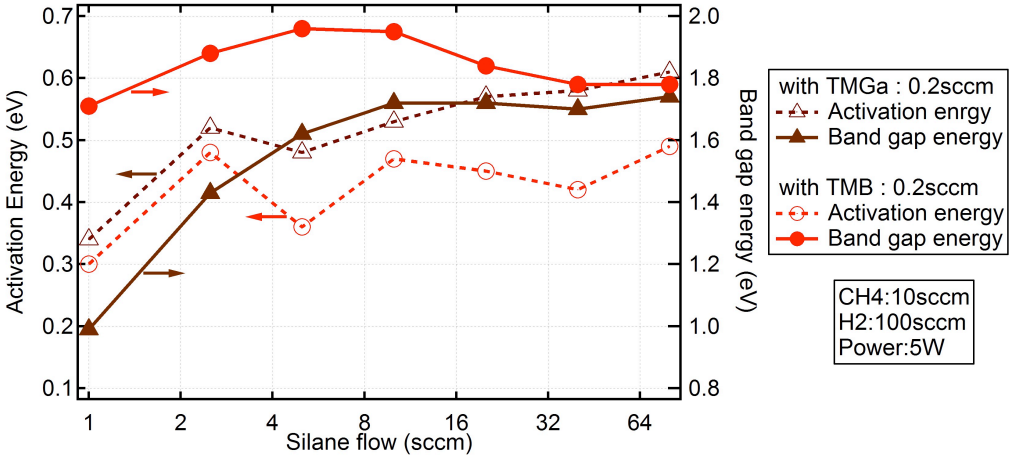

Figure 18: Band gap and activation energies of p-(a-SiC:H) layers doped by TMGa or TMB with varying SiH_4 flow.

Poor V_{OC} values for low SiH_4 flows are obtained for the solar cells with Ga and B, as seen in figure 19. V_{OC} saturation with Gallium doping is only attained for 20 sccm SiH_4 flow. Solar cells prepared with p-(a-SiC:H) layers doped with Ga show again lower V_{OC} but following the same trends as with boron doping except for the highest silane flow: there, the same drop as seen already in figure 15 is observed.

The activation energy was too high and the band gap too low for p-layers with Ga to provide a sufficiently high V_{OC}.

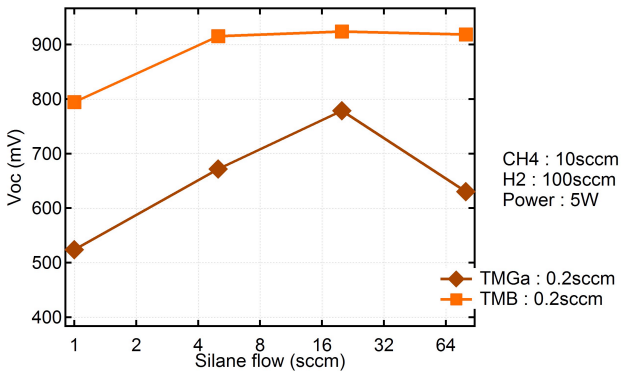

Figure 19: Open circuit voltage of two series of p-i-n solar cells with p-(a-SiC:H) layers doped by TMGa or TMB with varying SiH_4 flow.

With lowest SiH_4 flow for p-layers EQE for the solar cell is reduced on the entire spectrum and demonstrates amplification when a bias voltage appied, as observed in the previous section, too. The highest SiH_4 flow deposited with Ga dopant is also observed with amplified EQE at short wavelengths as showed in figure 20 a). Increased silane flow leads to a better EQE for the most of the spectrum, however, with B the increase in EQE is limited in short wavelengths as you can see in figure 20 b). These curves show that Ga in a p-layer causes higher absorption in the layer, and not only the short wavelengths.

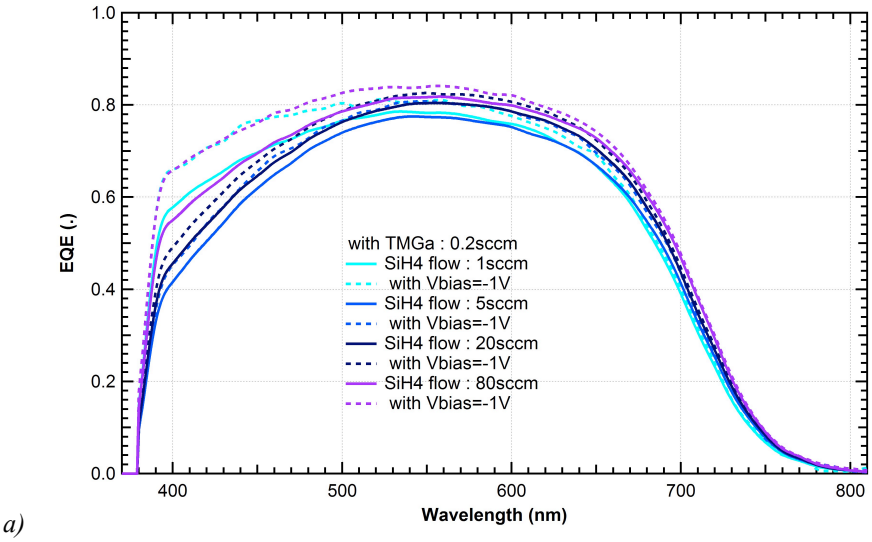

a)

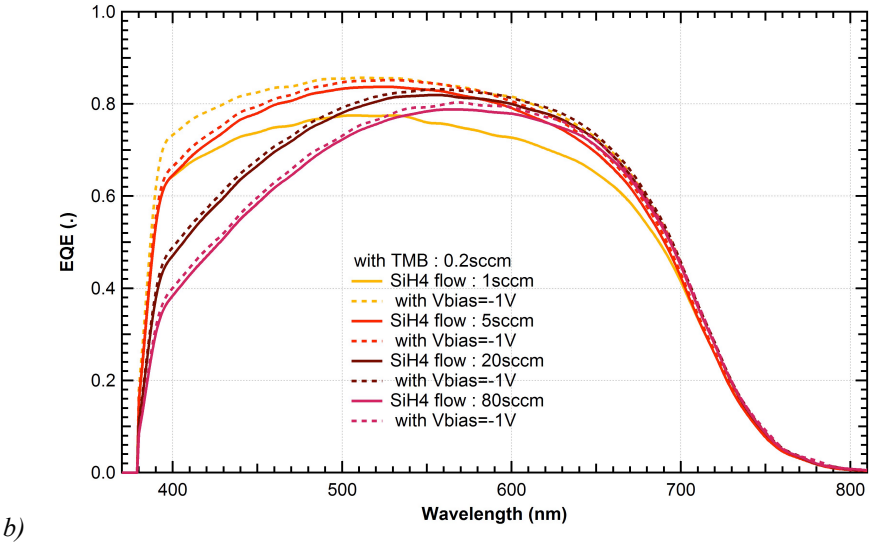

b)

Figure 20: External quantum efficiency curves of p-i-n solar cells with p-(a-SiC:H) layers doped in a) by TMGa or in b) by TMB with varying SiH_4 flow.

Furthermore, when a bias voltage of -1 V is applied to the cells, the ones with p-layers deposited in lowest SiH_4 dilution demonstrated much higher EQE at short wavelengths. This indicates a low internal electric field. The same effect is, however, encountered with the solar cell containing the highest SiH_4 dilution in its p-layer deposition doped with TMGa.

In the case of B, the highest EQE of incident light is obtained for the cell with 5 sccm SiH_4 flow in p-layer deposition, whereas, the best V_{OC} for the cell with 20 sccm SiH_4 processed with p-layer. For Ga, the best EQE is obtained with solar cells containing 80 sccm in p-layer and the best V_{OC} with the one containing 20 sccm.

4.6.1. With vs without methane

In this section, results obtained with layers and cells reported in the previous two sections will be compared regarding the influence of methane in the deposition of p-layers, instead of the dopants.

Similarly to [Tawada, 1982_jap] and [Wang, 1999], the introduction of carbon atoms in boron-doped layers leads to a shift of E_{gap} to higher energy levels particularly at low SiH_4 flows. As plotted in figure 21 a) et b), layers containing Ga, like with B, show a band gap widening when carbon is inserted, particularly for the lowest silane flow. The trend of the E_{gap} of Ga-doped carbide layers is very similar to the one of B-doped layers without

additional CH_4, at a slightly higher level. However, increase in activation energy of p-layers containing Ga is less pronounced if no additional carbide source was present in the deposition, still, following a similar trend. Likewise, with B dopant changes in E_{act} are to the same direction but include lower minimum values and higher maximums when CH_4 is used. As a result of the shift at higher energies of E_{gap} and to slightly lower activation energies, a-SiC:H layers are better suited for their application as window layer in p-i-n solar cells rather than a-Si:H for both dopant.

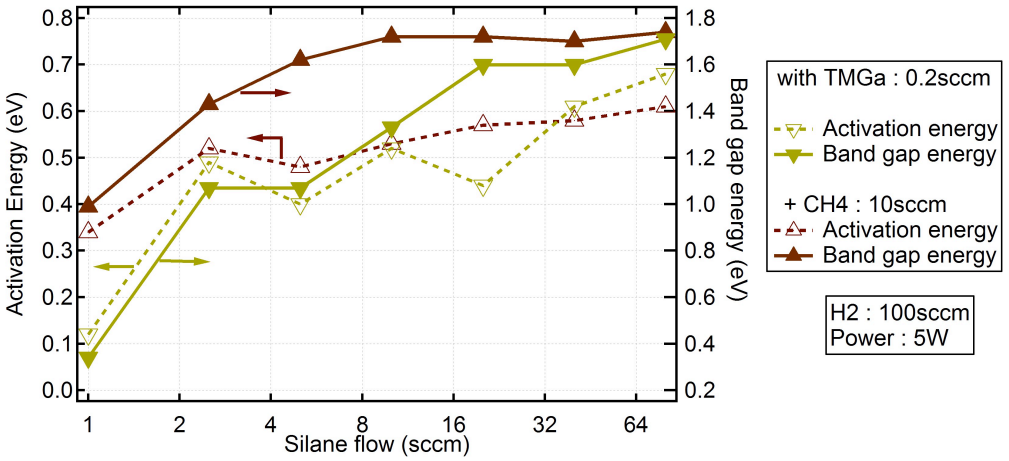

a) p-(a-Si:H) and p-(a-SiC:H) with Ga dopant

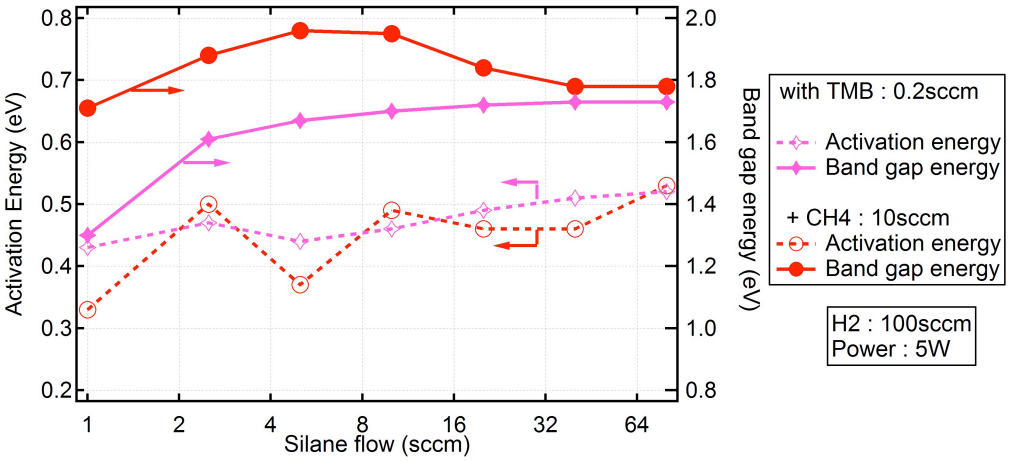

b) p-(a-Si:H) and p-(a-SiC:H) with Ga dopant

Figure 21: Band gap and activation energies of two series of p-(a-Si:H) and two series of p-(a-SiC:H) layers doped in a) by TMGa and in b) by TMB.

Correspondingly, solar cells with the lowest silane flow used for p-layers provide a higher V_{OC} than solar cells with a p-layer without carbon, as can be seen in figure 22. For higher silane flows, the V_{OC} values are similar. This is the case for solar cells containing any of two dopants. Better electrical properties thanks to B dopant than Ga is demonstrated yet again with higher open circuit voltages.

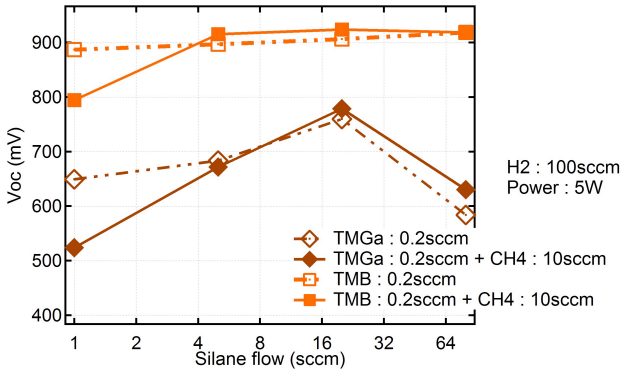

Figure 22: Open circuit voltages of two series of two series of p-i-n solar cells with p-(a-Si:H) layers and two series with p-(a-SiC:H) layers doped by TMGa or TMB.

External quantum efficiency curves of a-Si:H solar cells containing p-layers with or without methane are displayed in figure 23 a) for 5 sccm, b) 20 sccm and c) 80 sccm of SiH_4. With the increasing silane flow for the p-layer an opposite behaviour is observed between solar cells containing Ga or B dopant, as mentioned in the previous two sections. Obviously, adding CH_4 in the p-layer deposition results in solar cells with higher EQE thanks to less parasitic absorption, especially if low silane flow used. However, the gain in EQE for the solar cells with Ga is not observed only at short wavelengths but on the entire light spectrum. Band gap energies of p-layers deposited with 80 sccm SiH_4 for both dopant were resulted in the same order if CH_4 was used or not. Similarly, EQE of solar cells with p-layers containing C or not are in the same range relative to two other depositions, except the p-(a-Si:H) doped with TMGa shows a siginificant difference in short wavelengths. Additionally, both cells with p-(a-Si:H) and p-(a-SiC:H) layers doped with TMGa show a strong increase in the EQE at short wavelengths if a bias voltage is applied. Higher silane flow would decrease the dopant ratio in the p-layer, which leads to weaker internal electric field. Thus, for biased solar cell with -1 V between two contacts the collection of the electron-hole pairs is eased as observed in EQE curves.

Finally using doped a-SiC:H for p-layer lead to better EQE for p-i-n solar cells. Though, the ones with p-layers containing the highest SiH_4 flow the increase is much higher with Ga dopant than with B, particularly when CH_4 is also used.

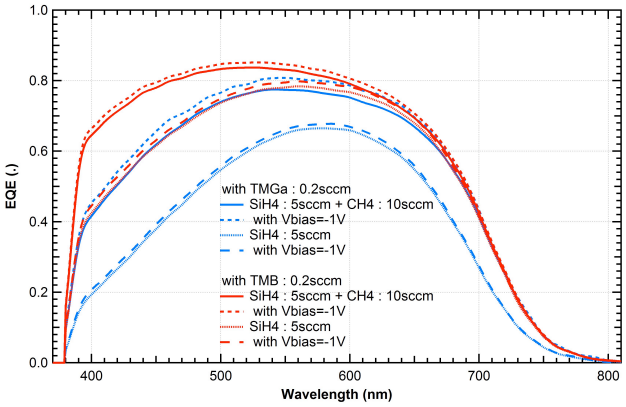

a) SiH_4 flow of 5 sccm

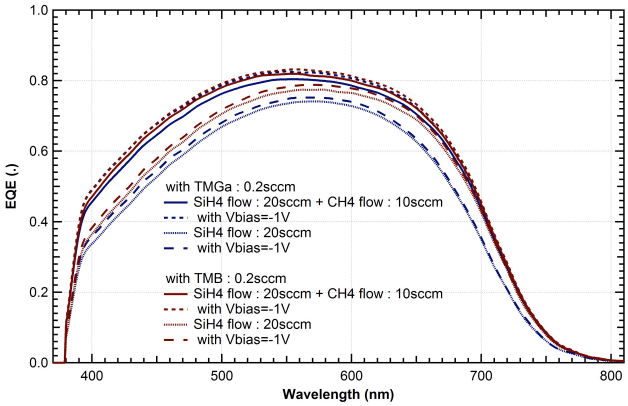

b) SiH_4 flow of 20 sccm

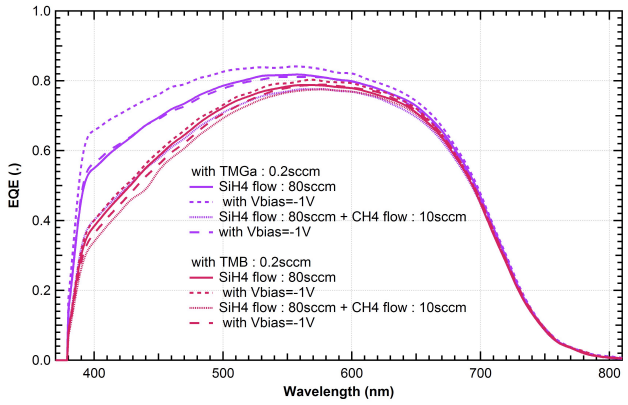

c) SiH_4 flow of 80 sccm

Figure 23: External quantum efficiency curves of two series of p-i-n solar cells with p-(a-Si:H) layers and two series with p-(a-SiC:H) layers doped by TMGa or TMB, and in a) with 5 sccm SiH_4 flow, in b) with 20 sccm SiH_4 flow and in c) with 80 sccm SiH_4 flow.

4.7. Silane / Methane ratio series of p-(a-SiC:H)

In this section, the effects of varying the silane to methane ratio on the p-layers electrical and optical characteristics are investigated. For these series a notably lower H_2 flow than for other series was used (25.8 sccm). TMGa and TMB flows were kept at 0.2 sccm. SiH_4 flow was 1, 2, 4, 6, 8, 9, 10 sccm, while CH_4 was decreased by the same order keeping their total flow equal to 10 sccm. However, for Ga- and B-doped a-SiC:H layers deposited with SiH_4 flow of 1 sccm, resulted probably in too resistive layers due to lack of silicon among the large amount of C, hence did not result in successful dark conductivity measurements. These points were excluded from this report. Anyhow, the effects of high CH_4 dilution of SiH_4 will be observed, particularly, in external quantum efficiencies of solar cells containing these layers as window layer.

The band gap of the B- and Ga-doped layers narrows strongly with increasing ratios of SiH_4 to CH_4, as shown in figure 24, which follows previous results [Wang, 1999] [Tawada, 1982] for B-doped a-SiC:H. The activation energy of TMB doped p-layer decreases with E_{gap}. Above a SiH_4 / CH_4 flow ratio of 4, the activation energy increases again and EF tends towards the middle of the band gap.

On the other hand, E_{act} of p-(a-SiC:H) layers doped with Ga decreases very slowly by less than 0.02 eV for increasing SiH_4 to CH_4 ratio, while the band gap follows the trend of boron doped layers. This indicates the shift of the Fermi level towards the mid gap with increasing SiH_4 to CH_4 ratio. From this layer analysis it seems that optimum SiH_4 to CH_4 ratio is higher for boron-doped as compared to gallium-doped layers.

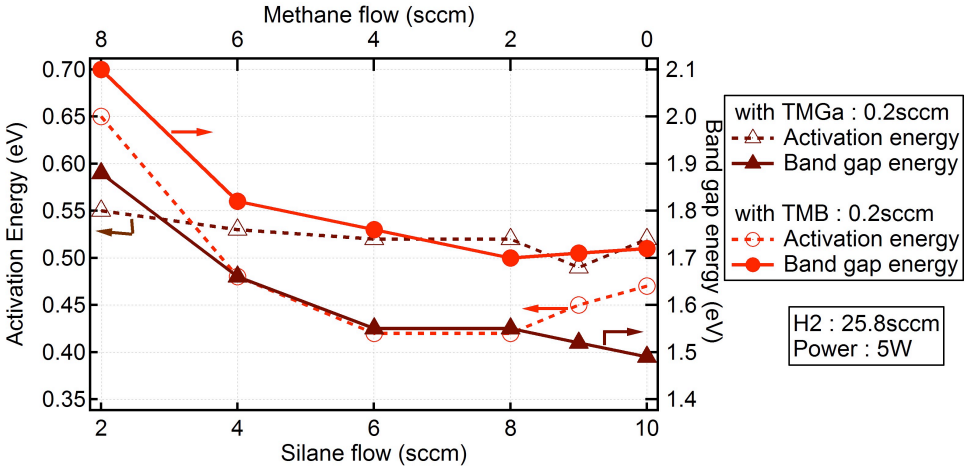

Figure 24: Band gap and activation energies of p-(a-SiC:H) layers doped by TMGa or TMB with varying ratio of SiH_4 to CH_4, their total equal to 10 sccm.

Two series of p-i-n solar cells are deposited including the p-(a-SiC:H) layers with varying silane to methane flow ratio, as described above. V_{OC} of these solar cells increases with silane/methane flow ratio until reaching saturation, as can be seen in figure 25. Anyway, V_{OC} for solar cells containing Ga dopant is observed increasing with higher ratios of SiH_4 to CH_4 even though a slow shift of the Fermi level towards mid gap was found earlier for their p-layers, which is expected to lead to a reduction of the built-in voltage in the solar cell thus to lower V_{OC}. The reason for it is not clear and needs further studies for understanding of the phenomena.

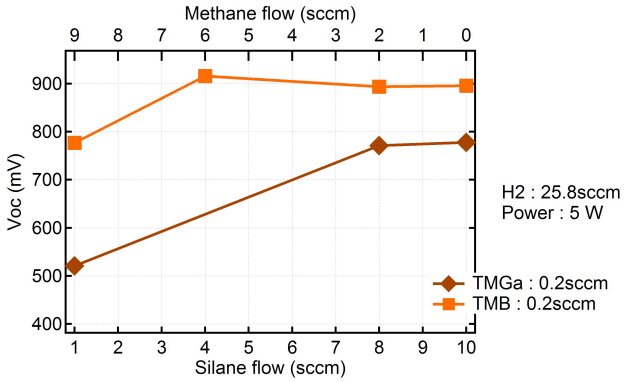

Figure 25: Open circuit voltages of p-i-n solar cells with p-(a-SiC:H) layers doped by TMGa or TMB with varying ratio of SiH_4 to CH_4, their total equal to 10 sccm.

TMB with varying ratio of SiH_4 to CH_4, their total equal to 10 sccm, deposited on Z5/2 7‘. The sample containing a p-layer prepared with 4 sccm SiH_4 and 6 sccm CH_4 did not result in working solar cells, probably due to a problem during deposition.

EQE curves of these p-i-n solar cells are mostly governed by strong parasitic absorption of the p-layers at short wavelengths, as displayed for solar cells with Ga and B dopants in figure 26 a) and b), respectively. For boron doping, only the solar cell containing a dilution of 66.7% SiH_4 in CH_4 (4:6) of the p-layer shows significantly higher EQE. The same solar cell had the highest V_{OC} too.

The charge collection of the cell with a p-layer deposited with 11% silane in methane (1:9) is poor both for boron and gallium doping. These two solar cells contain a p-layer, where too low silane flow was used and conductivity measurements were not successful, as told in the beginning of present section. Considering that these layers are not anymore diluted a-Si:H layers but mostly carbide layers with some silicon inserted in the network. Hence, it is most presumably that these layers, when incorporated in p-i-n solar cell structures, cannot provide a sufficient electric field.

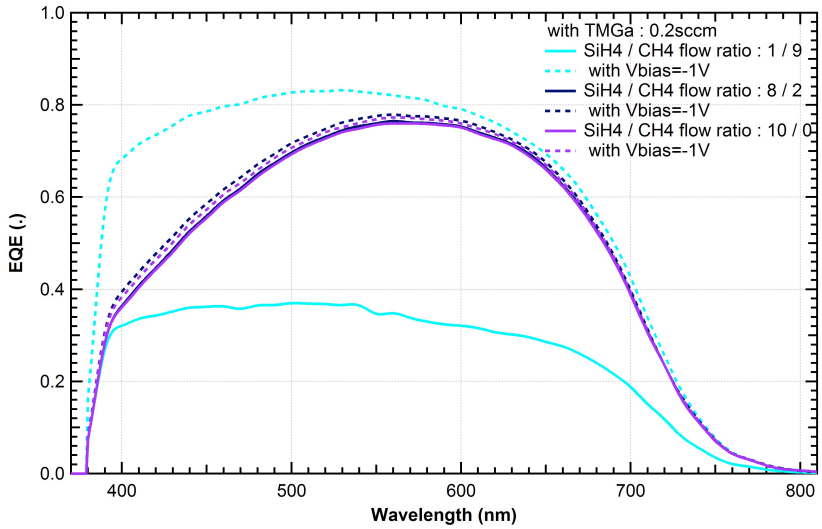

a)

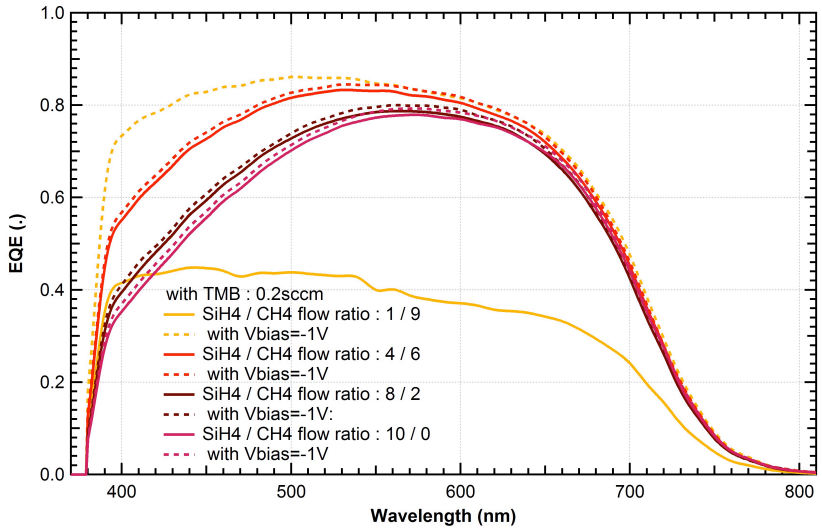

b)

Figure 26: External quantum efficiency curves of p-i-n solar cells with p-(a-SiC:H) layers doped in a) by TMGa or in b) by TMB with varying ratio of SiH_4 to CH_4, their total being constant at 10 sccm.

4.8. Temperature series

A deposition temperature study was also carried out with series of p-(a-SiC:H) layers as well as with series of p-i-n solar cells, where the deposition temperature of the i-layer was varied. The latter is aiming to compare the boron-tailing effect with two dopants, TMGa and TMB.

4.8.1. p-layer deposition temperature series of p-(a-SiC:H)

Investigated p-layers were deposited with a gas mixture including 0.2 sccm of TMGa or TMB, 4 sccm SiH_4, 8 sccm CH_4, and 12.9 sccm H_2 at 5 W. The deposition temperature was increased with one step in the middle from 140 °C to 260 °C. Dark conductivity measurements for layers doped with TMB ended up with highly reduced E_{act} when the deposition temperature is increased from 140 °C to 200 °C; and the decrease between a deposition at 200 °C and 260 °C is well below the change for lower temperatures, as displayed in figure 26.

For layers doped with Ga, between the lowest and highest deposition temperatures activation energy decreased homogenously by 0.15 eV in total and the E_{gap} by about 2.5 eV.

With B doping, the activation energy decrease with temperature is stronger (0.25 eV in total), but the band gap drop is smaller (0.15eV).

The narrowing of the band gap with the increasing deposition temperature for TMB doped a-SiC:H layers can be explained by the reduction of the hydrogen content in the deposited layer as it was demonstrated in [Platz, 1998]. A similar decrease is observed in figure 27, with the TMGa doping in this series the same explanation can describe the change, however this needs further measurements of the layer composition to conclude definitely.

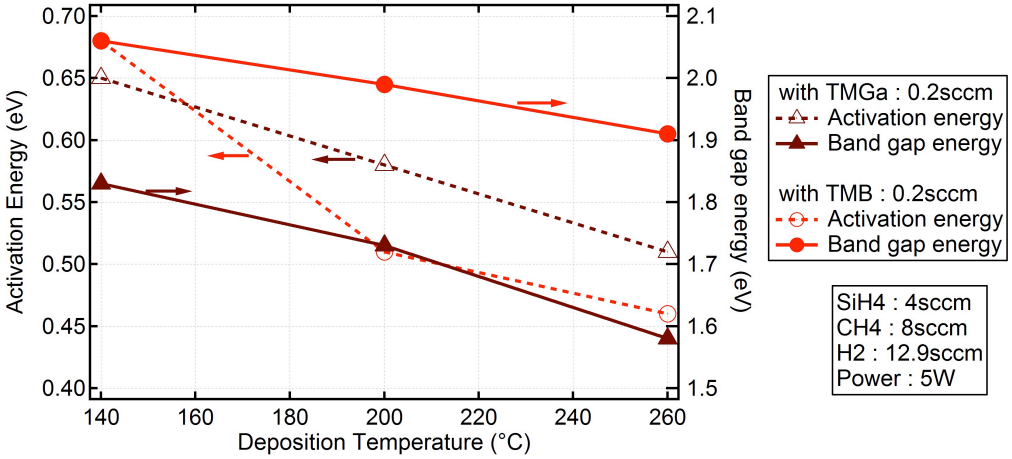

Figure 27: Band gap and activation energies of p-(a-SiC:H) layers doped by TMGa or TMB with varying deposition temperature.

4.8.2. i-layer deposition temperature series of p-i-n a-Si:H solar cells

In this series, deposition parameters were kept constant for p-layers with 0.2 sccm dopant, 20 sccm SiH_4, 10 sccm CH_4 and 100 sccm H_2. Only the deposition temperature of i-layers is increased for two series of p-i-n a-Si:H solar cells prepared with Ga or B dopant, precisely at 200 °C, 220 °C, 240 °C and 260 °C.

Open circuit voltages of p-i-n a-SiC:H solar cells are displayed according to the deposition temperature of their i-layers in figure 28. In case of boron doping, the Voc decreases with increasing temperature as expected due to band gap narrowing due to less hydrogen content deposited in the layer [Platz, 1998]. Interestingly, cells with gallium-doped p-layers show an increase in V_{OC} when the i-layer deposition temperature is raised. Only at temperatures above 240 °C it reduced notably. The reason for the Voc increase that is expected to decrease due to the lower band gap of the i-layer, is not clear. Possibly, gallium dopants are activated by annealing at 240 °C, though, further study is needed to investigate the layer's composition.

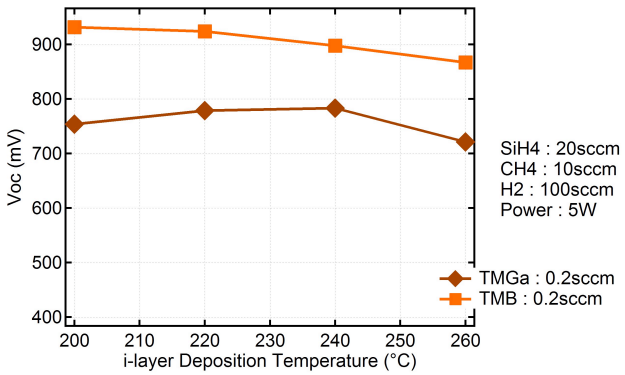

Figure 28: Open circuit voltages of two series of p-i-n solar cells with p-(a-SiC:H) layers doped by TMGa or TMB with varying i-layer deposition temperature.

Increasing the deposition temperature of the i-layer, in solar cells deposited according the same parameters with TMGa or TMB doping, leads to a shift of the EQE curves to higher wavelengths, as plotted in figure 29 a) and b). Meanwhile the absorption at short wavelengths is better with i-layers deposited at low temperatures and at long wavelengths is better with the ones deposited at high temperatures, the switch taking place around 550nm. Yet large band gap reached with low deposition temperatures of a-Si:H, implies a better absorption in long wavelengths.

The solar cell containing Ga in p-layer and whose i-layer was deposited at 260 °C, has particularly higher EQE than the others on the entire light spectrum. It was at the same time the one with the lowest V_{OC} value of the series. Moreover it presents notably the boron-tailing effect unlike all other samples. Having this effect only with Ga dopant, and even there less pronounced than expected, was a surprising result for the series of solar cells with varying i-layer deposition temperature. Though with B dopant the effect is not encountered in this series, which may be an indication that boron-tailing is evitable according to the deposition parameters. In fact p-layers of the solar cells presented here are deposited with different conditions as compared to the standard p-i-n recipe.

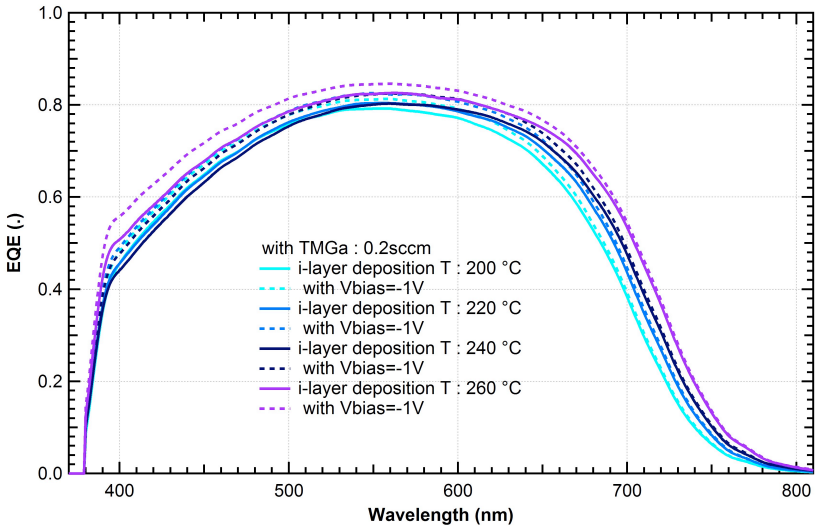

a)

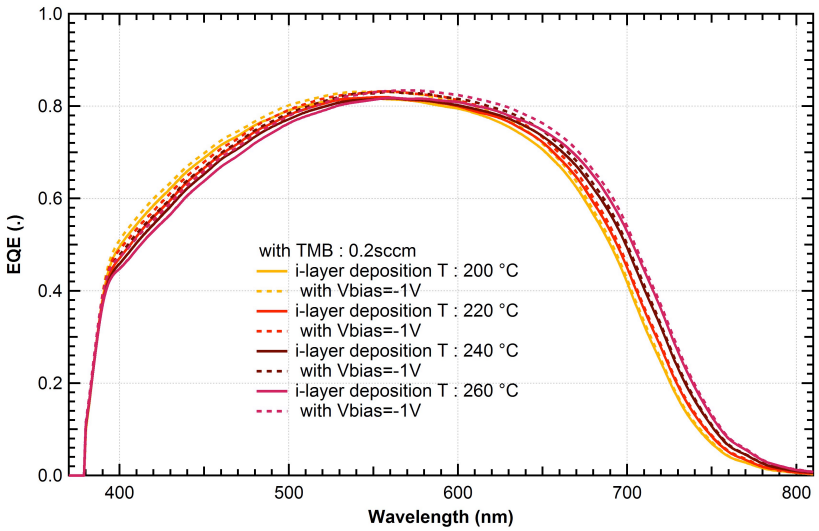

b)

Figure 29: External quantum efficiency curves of p-i-n solar cells with p-(a-SiC:H) layers doped in a) by TMGa or in b) by TMB with varying i-layer deposition temperature.

4.9. p-layer thickness series of p-i-n a-SiC:H solar cells

As the final series within this project, the cells with the higest V_{OC} for each dopant, discussed in section 4.6., were deposited with same parameters except with a thinner p-layer (7 nm instead of 20 nm). Characteristic values of these four solar cells are presented in table 2. The changes in J_{SC} for the ones containing B in different thicknesses are very similar to the standard cell case presented in section 4.2.

Tablo 2: Efficiency, open circuit voltage, short circuit current density and fill factor values for two solar cells with the best Voc obtained with TMGa and TMB doping in this project and two other deposited with the same recipe but thinner p-layer, 7 nm instead of 20 nm

p-i-n a-SiC:H solar cell with	*Efficiency*	*V_{OC}*	*J_{SC}*	*Fill Factor*
7 nm p-layer with TMGa	*7.02 %*	*619.8 mV*	*16.21 mA/cm^2*	*62.25*
20 nm p-layer with TMGa	*5.83 %*	*778.8 mV*	*14.60 mA/cm^2*	*46.21*
7 nm p-layer with TMB	*11.61 %*	*913.7 mV*	*15.76 mA/cm^2*	*73.24*
20 nm p-layer with TMB	*10.6 %*	*924 mV*	*14.94 mA/cm^2*	*72.99*

The conversion efficiencies of the solar cells containing Ga dopant are lower than with B dopant; especially with 20 nm thick p-layer it is almost half of what is obtained with TMB doped layers due to lower fill factor and V_{OC}. The reduction of the thickness of p-layers in solar cells leads also in a higher short circuit current with TMGa doping and in a lower V_{OC}. Though, J_{sc} collected with solar cells containing Ga in 7 nm thick p-layers is almost 1 mA/cm^2 higher than with B, meaning that the absorption in Ga doped layers is lower than the ones doped TMB. As for the decrease in V_{OC} is observed more strongly if TMGa is used for the p-layer of the solar cell rather than TMB, as seen also in figure 30. That indicates high dependence of the internal electric field on the thickness of p-layer if Ga dopant is used.

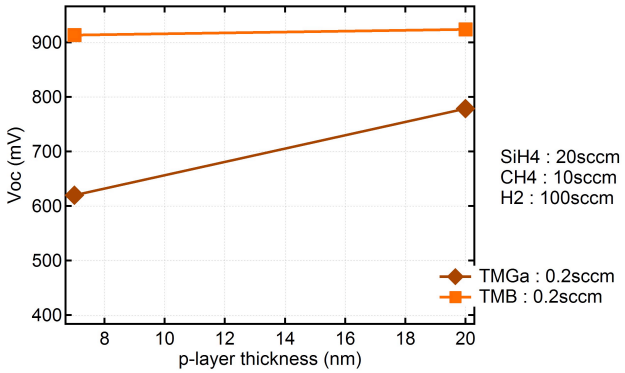

Figure 30: Open circuit voltages of p-i-n solar cells with p-(a-SiC:H) layers doped by TMGa or TMB with varyied p-layer thickness.

Obviously, parasitic absorption at short wavelengths is strongly enhanced with thicker window layer, as displayed in figure 31, on the contrary of the great gain in V_{OC} discussed previously. It is due to the decreased penetration depth of the incident photon with a thin p-layer at the front of the solar cell, thus, reduced probability of being absorbed in the p-layer before reaching the active i-layer. Above all, reducing the thickness of TMGa doped p-layer in a p-i-n solar cell presents much higher EQE at the short wavelengths than the one with thinner B doped p-layer. It is, however, quite opposite to other results obtained with solar cells containing Ga. Possibly, this is due to different doping effect of boron and gallium, but more likely is an experimental error, as too thin p-layer gives similar results.

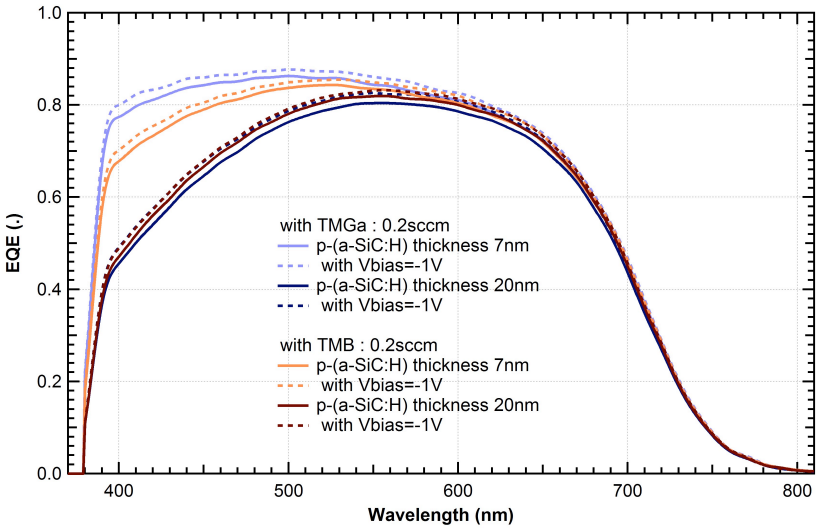

Figure 31: External quantum efficiency curves of p-i-n solar cells with p-(a-SiC:H) layers doped by TMGa or TMB with varyied p-layer thickness.

5. Conclusion

Mostly, similiar changes but much more pronounced effects, either positevly or negatively, are observed in optical and electrical characteristics of amorphous silicon layers deposited with Ga than with B dopant. However, boron doping shows better performance in amorphous silicon solar cells, at least with given hardware limitations, both optically and electrically In particular, band gap narrowing by doping was more pronounced with gallium than with boron, especially at higher deposition temperatures.

Largest band gaps are obtained with a gas mixture of 2 sccm SiH_4, 8 sccm CH_4, 25.8 sccm H_2 and 0.2 sccm doping gas, and are 1.88 eV with Ga and 2.10 eV with B dopant. And lowest dark conductivity activation energies resulted with the lowest silane gas flows with a dilution of 1% in hydrogen for Ga dopant and for B with an additional CH_4 flow of 10 sccm was used. The minima for Ga and B are very similar and equal to 0.34 eV and to 0.33 eV, respectively.

Deposition power variations for p-layers resulted in both optical and electrical improvements with increased power.

Low doping gas flow in the deposition of p-layers lead to a much stronger band gap narrowing with Ga than with B. Increasing TMB gas flow results in better doping effects thanks to the homogeneous shift of Fermi level away the mid gap. On the other hand, Ga as a dopant must be used in much less amounts to produce a conductive p-layer with wide band gap. When incorporated in p-i-n solar cells, increasing the doping in p-layers resulted in a reduction of V_{OC}, especially with Ga, due to band gap narrowing. Additionally, higher TMGa flows resulted in strong parasitic absorption leading to lower EQE over the whole spectrum. In contrast, strong boron doping only leads to an increase of the parasitic absorption at short wavelengths.

The silane flow was varied for doped amorphous silicon, but also for amorphous silicon carbide. A clear increase of the band gap energy is observed for both dopants, for higher silane flows and, also, when carbon is added. Activation energy with both dopants is slightly reduced if lower silane flow is used for p-layer deposition. When deposited within p-i-n solar cells, parasitic absorption in p-layers is contrarily affected with increased silane flow for two dopants; strongly reduced if Ga doped and increased with B.

With both dopants, V_{OC} is slightly increased with p-(a-SiC:H) as compared to p-(a-Si:H) layers. The highest V_{OC} values obtained within this project are 778.8 mV and 924 mV for solar cells with Ga and with B, respectively. In these cases, the p-layers have been deposited with 20 sccm SiH_4, 10 sccm CH_4, 100 sccm H_2 and 0.2 sccm doping gas at 5 W and 200 °C.

Increasing the i-layer deposition temperature up to 260°C did not lead to boron or gallium tailing characteristics, when p-layer was deposited with the recipe resulted in best V_{OC}. However, a strong current increase could be observed with increasing temperature due to a lower band gap.

Lastly, solar cells reporting the best V_{OC} were once more deposited with thinner p-layers, which resulted in a significant gain in the EQE at short wavelengths. Thus, short circuit current is increased. This effect is much more pronounced with Ga than with B. V_{OC} values are reduced with the p-layer thickness, again to larger extent for gallium doping than for boron doping. To conclude, gallium leads to similar trends like boron as a p-dopant in hydrogenated amorphous silicon layers. However, when these layers are incorporated into a-Si:H solar cells, the cells with gallium showed poorer performance. Namely, the band gap narrowing due to gallium doping is an issue and leads to poor V_{OC}. However, the highest V_{OC} values have been found with the lowest possible gallium flows. This indicates that p-layers that are more suited for a-Si:H solar cells could be obtained with lower doping ratios. To clearify this, further experiments are necessary for example by using a bubbler for TMGa dilution with a carrier gas.

6. Acknowledgement

I would like to thank Prof. Christophe Ballif for giving me the chance to join PV-Lab for the master project, and his group for their well-coming attitude as well as ambitious working environment.

I am very grateful to Michael Stuckelberger for his advices during the project.

Finally, for their fully support I wish to mention my gratitude to my family and Joachim Kunz.

7. Bibliography

Carlson, D.E. and Wronski, C.R., "Amorphous silicon solar cell," Applied Physics Letters. Vol. 28, No. 11, 671 – 673, (1976)

Chittick, R.C., Alexander, J.H. and Sterling, H.F., "The Preparation and Properties of Amorphous Silicon," J. Electrochem. Sac. Vol. 116, No. 1, 77 – 81, (1969)

Ding, L., "Low-Pressure Chemical Vapor Deposited Zinc Oxide Films : Toward Decoupled Opto-Electrical and Morphological Properties for more Efficient Electrodes", Thesis n°6010, EPFL, (2013)

Green, M. A., Emery, K., Hishikawa, Y., Warta, W., and E. D. Dunlop, "Solar cell efficiency tables (version 43)", Prog. Photovolt: Res. Appl. Vol. 22, 1 – 9, (2013)

Goetzberger, A., Luther, J., and Willeke, G., "Solar cells: past, present, future", Solar Energy Materials & Solar Cells Vol 74, 1 – 11, (2002)

Keppner, H., et al., „Microcrystalline silicon andmicromorph tandem solar cells", Appl. Phys. A Vol. 69, 169 – 177, (1999)

Li, Y.-M., et al., "An exploratory survey of p-layers for a-Si:H solar cells", Mat. Res. Soc. Symp. Proc. Vol. 336, 663 – 668, (1994)

Lloret, A., et al., "Hydrogenated Amorphous Silicon p-Doping with Diborane, Trimethylboron and Trimethylgallium", Appl. Phys. A Vol. 55, 573 – 581, (1992)

Meier, J., Flückiger, R., Keppner, H., and Shah, A., „ Complete microcrystalline pin solar cell—Crystalline or amorphous cell behavior?", Applied Physics Letters Vol. 65, No. 7, 860 – 862, (1994)

Okamoto, H., et al, "Mobility lifetime product and interface property in amorphous silicon solar cells", Journal of Applied Physics Vol. 54, No. 6, 3236 – 3243, (1983)

Platz, R., et al., "Influence of excitation frequency, temperature, and hydrogen dilution on the stability of plasma enhanced chemical vapor deposited a- Si:H", Journal of Applied Physics Vol. 84, No. 7, 3949 – 3953, (1998)

SFOE, "Le recensement du marché de l'énergie solaire en 2012: Extrait de la statistique suisse des énergies renouvelables", (2013)

Shah, A.V. (Ed.), "Thin-film silicon solar cells", Lausannee: EPFL Press, (2010)

Spear, W.E., and Le Comber, P.G., "Substitutional doping of amorphous silicon", Solid State Communications, Vol. 17, 1193 – 1196, (1975)

Staebler, D.L., and Wronski, C.R., "Reversible conductivity changes in discharge produced amorphous Si", Applied Physics Letters Vol. 31, No. 4, 292 – 294, (1977)

Stuckelberger, M., Riesen, Y., Perruche, B., Despeisse, M., Wyrsch, N., Ballif, C., "Charge collection in amorphous silicon solar cells: Cell analysis and simulation of high-efficiency *pin* devices", Journal of Non-Crystalline Solids, (2011)

Tarui, H., et al, "High-quality p-type a-SiC films obtained by using a new doping gas of $B(CH_3)_3$, Japanes Journal of Applied Physics Vol. 28, No. 12, 2436 – 2440, (1989)

Tawada, Y., et al., "aSiC:H/aSi:H heterojunction solar cell having more than 7.1% conversion efficiency", Applied Physics Letters Vol.39, No. 3, 237 - 239, (1981)

Tawada, Y., et al., "Hydrogenated amorphous silicon carbide as window material for high efficiency a-Si solar cells", Solar Energy Materials Vol. 6, 299-315, (1982)

Wang, L., et al., "The influence of the growth conditions on the structural and optical properties of hydrogenated amorphous silicon carbide thin films", Journal of Alloys and Compounds Vol. 290, 273 – 278, (1999)